DIELECTROPHORETIC TRAPPING OF 3D-DNA ORIGAMIS

Janne Saastamoinen

Master's thesis
University of Jyväskylä, Department of Physics
26.08.2015
Supervisors: Jussi Toppari
Boxuan Shen

Kolmiulotteisten DNA-origamien dielektroforeettinen vangitseminen

DNA-molekyylien 1980-luvulta lähtien Nadrian Seemanin uraauurtavan tutkimustyön myötä yleistynyt tutkimus ja käyttäminen erilaisissa nanoteknologian sovelluksissa perustuu erityisesti sen kykyyn itsejärjestyä spesifisen emäspariutumisensa ansiosta. Tätä itsejärjestyvyyttä hyväksikäyttämällä etukäteen suunnitelluilla emässekvensseillä varustetuista DNA-juosteista voidaan muodostaa koko ajan monimutkaisempia nanoskaalan rakenteita. Ensimmäisistä kaksiulotteisista rakenteista ja kuvioista on pystytty siirtymään kolmiulotteisiin hyödyntämällä DNA-juosteiden taipuisuutta yksinkertaisesti taittamalla kaksiulotteinen muoto kolmiulotteiseksi.

DNA-origamilla tarkoitetaan järjestelmää, jossa yksijuosteinen DNA-molekyyli on taiteltu tiettyyn ennaltamäärättyyn muotoon. Haluttua muotoa aproksimoidaan liitämällä yhteen samansuuntaisia DNA-kierteitä, joiden läpi kulkee koko rakenteen matkalta erillinen scaffold-juoste. Tämä juoste luo lisää linkkejä kierteiden välille ja liittää niiden irtonaiset päät yhteen. Rakennetta koossapitävien liitosjuosteiden (staple strands) avulla scaffold-juosteen taittumista pystytään ohjaamaan ja luomaan vastakkaissuuntaisista DNA-kierteistä koostuva kaksiulotteinen origami. Kolmiulotteinen origami muodostetaan taivuttamalla edellämainittua litteää, kaksiulotteista origamia siten, että se muodostaa itsensä kanssa kennomaisen hilarakenteen, jota koossapitämään lisätään kierteiden välille liitosjuosteita. Tätä perusrakennetta muokkaamalla voidaan tämän jälkeen saada aikaan haluttu kolmiulotteinen muoto origamille. Origamien ja muiden DNA-rakenteiden suunnitteluun käytetään tähän tarkoitukseen varta vasten tehtyjä tietokoneohjelmia, jolloin pystytään helposti luomaan oikea sekvenssi juosteille.

Kun sopiva DNA-origami on saatu valmistettua, täytyy sitä pystyä myös käsittelemään jollakin tavalla, jotta yksittäisten origamien ominaisuuksia voidaan tutkia. Yksi menetelmä, jota tähän tarkoitukseen voidaan käyttää on dielektroforeesi. Dielektroforeesissa polarisoituva kappale, joka voi olla joko neutraali tai varattu, liikkuu epähomogeenisessa sähkökentässä. Kappaleen vastakkaisille pinnoille indusoituu tällöin sähkökentän vaikutuksesta positiivinen ja negatiivinen varausjakauma, jotka vuorovaikuttavat sähkökentän kanssa ja saavat aikaan Coulombin lain mukaisen voiman. Koska dielektroforeesissa käytettävä sähkökenttä on epähomogeeninen, nämä voimat ovat erisuuruisia ja siten nettovoima on nollasta poikkeava aiheuttaen kappaleen liikkeen.

Dielektroforeesia voidaan käyttää ”vangitsemaan” näytteen partikkeleita elektrodien väliin. Tämä onnistuu lisäämällä elektrodien ympärille näytepartikkeleita sisältävää liuosta ja kytkemällä niiden välille sähkökenttä. DNA:n tapauksessa käytetyn sähkökentän tulee olla AC-kenttä, sillä molekyylin negatiivisesta varauksesta johtuen kaikki molekyylit liikkuisivat muutoin positiiviselle elektrodille sen sijaan, että ne sijoittautuisivat keskelle elektrodien välillä olevaa aukkoa. Jos näytteen permittiivisyys on sopiva, partikkelit liikkuvat kohti elektrodien välissä keskellä sijaitsevaa sähkökentän maksimia ja jäävät paikalleen. Dielektroforeettisen voiman lisäksi molekyylien liikkeeseen näyteliuoksessa vaikuttavat sekä termiset voimat että satunnainen Brownin liike, joka pahimmillaan voi jo itsessään olla dielektroforeettista voimaa suurempi ja estää vangitsemisen. Tästä johtuen on erityisen tärkeää, että vangittaville partikkeleille Brownin satunnaisvoima on tarpeeksi pieni ja että käytetty näyteliuos on johtavuusominaisuuksiltaan sopiva estääkseen lämpökonvektioiden vaikutukset vangitsemiseen. DNA-rakenteiden tapauksessa dielektroforeettista vangitsemista voidaan hyödyntää esimerkiksi mitattaessa DNA:n sähkönjohtavuutta, sillä tällä menetelmällä voidaan suhteellisen yksinkertaisesti eristää yksittäinen partikkeli tutkittavaksi.

Tässä Pro gradu-tutkielmassa pyrittiin vangitsemaan noin 400 nm pitkiä ja noin 5-6 nm korkeita putkimaisia DNA-origameja 150-ja 400 nm aukolla varustettujen kullasta ja titaanista valmistettujen piidioksidilevyllä olevien nanoelektrodien väliin. Nämä elektrodit valmistettiin Nanotiedekeskuksen puhdastiloissa elektronisuihkulitografiaa ja suurtyhjiöhöyrystystä käyttämällä. Näytteitä valmistettiin koko aikana yhteensä 101 kappaletta. Näistä 50:lle käytettiin 150 nm aukolla olevaa elektrodia ja lopuille 400 nm aukkoa. Dielektroforeettisen käsittelyn jälkeen näytteille suoritettiin kuvaus atomivoimamikroskoopilla, jotta voitiin varmistua siitä, oliko origameja saatu näytteessä vangittua. Onnistuneiden (vähintään yksi origami kiinnittyneenä kumpaankin

elektrodiin) vangitsemisten suhteen saannoksi saatiin 150 nm elektrodiaukolla noin 12 % ja 400 nm elektrodiaukolla noin 4 %, jolloin kokonaissaannoksi tuli noin 8 %.

Preface

The experimental and practical work for this Master's thesis was carried out at the Nanoscience Center of the Department of Physics, University of Jyväskylä during the years 2014-2015.

First and foremost I would like to thank my supervisors Doctor Jussi Toppari and Doctoral Student Boxuan Shen for their invaluable advice and guidance during the process of working on this thesis as well as for the skills and knowledge required to complete this work and for the chance to work as a trainee in the nanoelectronics group. I would also like to thank Doctoral Student Kosti Tapio for his insight and know-how as well as all the other personnel of the Nanoscience Center who have helped and adviced me when I've been in need of it. Additionally I want to thank my friends and family for their continuous support and encouragement during my studies.

Jyväskylä, August 2015

Janne Saastamoinen

Abstract

In this thesis three-dimensional tube-shaped DNA-origamis were dielectrophoretically trapped within lithographically fabricated nanoelectrodes. The origamis had been premade while the electrodes were fabricated specifically for these experiments with two different gapsizes, 150 nm and 400 nm. The aim of the work was to capture individual nanotubes in the gap between the electrodes by utilizing the dielectrophoretic forces present in the structure when a solution containing the origamis was put onto the electrodes and a voltage was applied.

It was observed during the experiments that the success of the dielectrophoretic trapping depended strongly on the trapping conditions. This caused the trapping to be somewhat challenging and it was also noticed that the electrode structure with the 400 nm gap particularly required patience in order to produce good results, since the origamis to be trapped were of the same size as the gap between the electrodes making the successful trapping problematic. Despite this, a sufficient amount of trapped single nanotubes were produced.

Contents

Chapter 1

Introduction

The development of nanotechnology has been accelerating ever since the basics upon which this field of research would later be built upon were presented by Richard Feynman in the 1950s. Starting from 1980s the interest in nanoscale applications that could utilize structures built from DNA-molecules began to gain popularity due to Nadrian Seeman's research on exploiting the specific self-assembly properties based on the base pairing of DNA in order to fabricate complex structures using single- and double-stranded DNA [1,2].

From these beginnings the use and study of DNA as a nanomaterial has grown steadily during the last 30 years because of the special characteristics of the molecule, such as good mechanical properties, self-assembly and small size, making it an appealing and versatile option for this purpose. Over the years DNA has been used to create a multitude of wildly varying constructs such as tubes, cubes or rectangles [3-9]. The invention of DNA 'origamis', first introduced by Paul W. K. Rothemund in 2006 [10], has been especially beneficial as it expands the use of the traditional 'building block' approach. This allows for even more possibilities in the assembly of complexes due to the different ways in which the DNA strands can be folded. This approach grants also the ability to create three-dimensionally folded origamis [10,11]. The basic two-dimensional origami consists of a long single strand of DNA which is folded and given shape by shorter strands of DNA keeping the structure together. Further folding of the 2D origami creates the shape of the 3D-origamis which were first presented by Douglas *et al* in 2009 [11]. Nanotubes which are used here in this thesis belong to this classification of 3D-origamis.

One of the main fields in which the use of DNA-nanostructures shows great promise is molecular electronics. However, due to the controversial results [12,13] on the conductivity of DNA and it's strong dependence on the conditions of measurement, one of the main focus points nowadays is the use of DNA as a base or a breadboard of sorts for electronic components instead of being the main material for the components themselves. In this regard the ability to attach other nanoparticles, such as gold, onto the DNA-molecules to create conjugated, functionalized and conducting structures is of great importance for the design of nanoscale components [14]. It is also possible to create the desired electrical properties for DNA by chemical treatment to achieve a suitable conductive coating across the molecule [14]. The main benefit of using DNA or other nanomaterials for electronics is the capability to bypass the problems presented by quantum mechanics for contemporary semiconductor technology. The significantly smaller size of molecular components as well as relatively lower costs, ease and speed of component fabrication compared modern silicon-based devices help to satisfy the evergrowing demand and need for more components on smaller circuits as well as Moore's law. Naturally there are still some issues that have to be overcome in the progress towards this, such as the dramatically increased heat generation from the large amount of devices that could be fit on the circuit area [14].

Due to the growing number of diverse self-assembled nanostructures being developed the need for methods for manipulating and controlling these objects arises, as well in order to complement the bottom-up approach of self-assembly with top-down techniques to handle the fabricated nano-objects. Not only does this enable the assembly and combination of even more complex nanoscale applications from smaller components but also benefits the analysis of individual nanoconstructs by offering ways to isolate and position them for the purposes of measurement. One such method which has been utilized in this thesis is dielectrophoretic (DEP) trapping where a polarizable particle moves in an inhomogenous electric field due to charge distributions induced upon it's surface by the electric field. This force is then used to 'trap' the particle between narrow fingertip-electrodes [2]. The properties, such as electrical conductivity for example, of the trapped and isolated particles can then be conveniently analyzed without the presence of any unnecessary substances. Dielectrophoretic trapping essentially combines the concepts of bottom-up and top-down in the sense that in this technique a top-down (lithography) fabricated electrode is used to manipulate bottom-up (self-assembly) built nanoparticles, or DNA-origamis in the case of this thesis, an approach which was mentioned earlier and one that will most likely have much potential for future development when nanoscale applications are carried to new levels of sophistication.

Chapter 2

Background

2.1 Self-assembly of DNA

DNA, or deoxyribonucleic acid consists of a chain of nucleotides that are bound together covalently with ester bonds between phosphate and deoxyribose which form the backbone of the DNA strand. These phosphodiester bonds form between 3' and 5' ends of the nucleotide, where 3' end contains a sugar (deoxyribose) and 5' end contains a phosphate. The nucleotide itself also contains a nitrogenous base in addition to the sugar and phosphate components [2].

The self-assembly of the DNA molecule is caused by the specific pairing of the bases (adenine (A), guanine (G), cytosine (C) and thymine (T)) between nucleotides according to the Watson-Crick-model. This is the most probable binding method in which adenine binds with thymine and cytosine binds with guanine via hydrogen bonds that are formed between single oxygen or nitrogen atoms and hydrogen-bound oxygen or nitrogen atoms. This base pairing is shown in figure 1 [15]. The size of one base is approximately 3.3 Å. Other pairings are also possible but as said, the Watson-Crick model is the most probable way of binding. Thus two complementary single-strand DNA-molecules can bind with each other in a predictable manner producing the DNA double helix structure. In this secondary structure of DNA the 3',5' -phosphodiester bonds of the two strands run in opposite directions, creating an antiparallel configuration. The distinctive pairing of the bases allows the process to be controlled and produces a great variety of nucleotide sequences to be used in fabricating complex self-assembled DNA-structures [2,14].

There exists several different 3D-conformations of the DNA double helix depending on the environment around the molecule. Most common ones of these are referred to as A-, B- and Z-DNA. The B-form is the most stable conformation and also the first one that was discovered. It has a right-handed helix whose diameter is approximately 2 nm with an average helical turn of 10.5 base pairs (bp) and a helix rise of about 0.34 nm per base pair. The A-form is similar to the B-form in being right-handed, however, its structural parameters have minor differences with diameter 2.6 nm, helical turn 11 bp and helix rise of 0.26 nm per bp. In addition, the A-form has a more tilted plane of base pairs respect to the helix axis (20^{o}) compared to the B-form (6^{o}) which contributes to the varying stabilities and electronic properties; for example the A-form requires less water molecules to surround it in order to remain stable in a solution than the B-form. In comparison, the Z-form is a left handed construct and has a zig-zag configuration in its sugar-phosphate backbone. It is also more elongated with a helical turn of 12 bp and a helix rise of 0.37 nm per bp. Models of A-, B- and Z-form are presented in figure 2 [2,16].

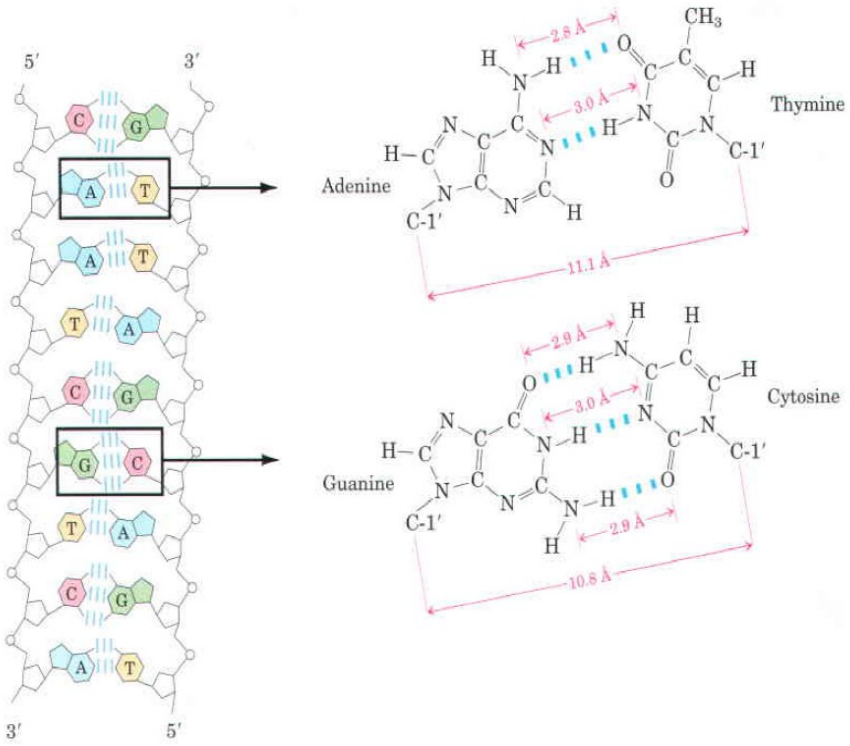

Figure 1: The base pairing between the single strands of DNA [15]

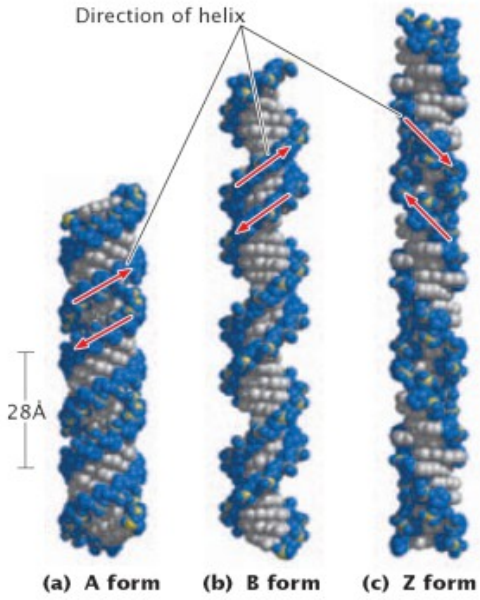

Figure 2: The A-, B-, and Z-conformations of the DNA double helix [16]

In addition to the useful self-assembly characteristics provided by the specific base pairing, DNA also has good mechanical properties with single-strand DNA being flexible and double-strand DNA being rigid in the scale of 50 nm. These combined with the small size of the molecule makes it a fascinating substance to be used in the 'bottom-up' fabrication. There are several possible

methods for utilizing DNA, such as using the building block approach for constructs like the TX-tiles or using a folding technique as in the case of DNA-origamis [1-11,17].

2.2 DNA-origamis

The term DNA-origami refers to a DNA structure in which a single strand of DNA is folded into a certain specific shape. To make the structure the general outline of the shape is approximated by using parallel DNA helices bound together by short staple strands crossing over from one helix to another. Long single scaffold-strand is folded over the structure in a raster pattern, creating more crossovers and binding the ends of the parallel helices together. There are gaps between the helices that may be caused by electrostatic interactions and the size of the gap depends on the spacing of the crossovers. The staple strands used to fold the single-stranded DNA molecule can also be used for functionalizing the structure, which can open the possibilities for using such origamis as breadboards for various nanoelectronic systems. As such, it is important to have a good understanding of the conductive properties of these DNA-structures [10].

The study of DNA as an organic building block took it's first steps in 1982 when Nadrian Seeman suggested the use of simple junction structures made from DNA as a way to construct complex geometric structures at the nanoscale [3]. The predictable nature of complementary base pair bonding between single-stranded DNA molecule allows for the 'programming' of DNA molecules to interact with each other in a predetermined way which would result in the desired assembly. However, because of the flexibility of DNA structures with only a single junction point there was no success in constructing higher-order architectures due to the lack of rigidity [5]. This problem was solved with the development of multiple-crossover motifs, of which the double crossover motif first reported in 1993 is of particular significance and still remains as the cornerstone in DNA nanotechnology [18]. This success initiated a series of developments which eventually led to the advent of the DNA origami. The use of a scaffold strand in DNA constructs was first employed by Yan *et al* in their process on constructing an aperiodic DNA lattice where DNA tiles were directly nucleated around the scaffold [19]. Another major breakthrough was to direct the folding of the scaffold strand by using a set of 'staple' strands to achieve a flat array consisting of antiparallel helices, first developed by Paul Rothemund [10]. When compared to previous approaches for DNA assembly these scaffolded DNA origamis had several advantages, such as small number of errors and defects and a higher yield. The synthesis is also quicker because there is no need to purify the oligonucleotides because there is no stoichiometric dependence [2,20].

The basic process of designing DNA-origamis involves five steps, starting with the building of a model which is approximately in the shape of the desired DNA-structure. An even number of parallel DNA-double helices is then used to fill out the shape, the helices being in sequential pairs and being an integer number of turns in length. These helices are idealized as cylinders. Crossover strands are then used in a periodic array to hold the overall helix structure together thus resulting in a rough model of the structure. The second step of the process is initiated with the folding of a single scaffold strand in a raster pattern, comprising one strand in each helix. This process creates additional crossovers in the structure (scaffold crossovers). The folding path of the long scaffold strand is restricted by the fact that it can only form a crossover in a location where it would be at a tangent point between helices [2,10,17].

After the design of the geometric model and the folding path of the scaffold are complete, the lists of DNA lengths and offsets along with the DNA sequence of the scaffold can be submitted into a computer program which then performs the third step of the overall design process. This step involves designing a set of 'staple strands' which create the periodic crossovers and act as Watson-Crick complements for the scaffold strand. At the crossovers the staple strands reverse direction causing them to be antiparallel. Because the DNA helix is asymmetric due to the major and minor

grooves, the periodic crossovers are balanced by arranging them in a glide symmetry so that in alternating columns of periodic crossovers the minor groove faces alternating directions [2].

The scaffold crossovers, however, are not balanced in a similar way. The fourth step consists of calculating the twist strain of the scaffold crossovers and adjusting their position by a minimal amount, typically by a single base pair. A nick occurs in the backbone of the structure in locations where two staples meet. These can be found on both top and bottom faces of the helices. In the final steps adjacent staples are merged across the nicks. This provides larger binding domains for the staples with the scaffold, resulting in higher binding specificity and binding energy. The seams may also be reinforced by creating additional merges and breaks to achieve staples which cross the seam. A schematic of a finished origami design carried out with the described steps is presented in figure 3[2,10].

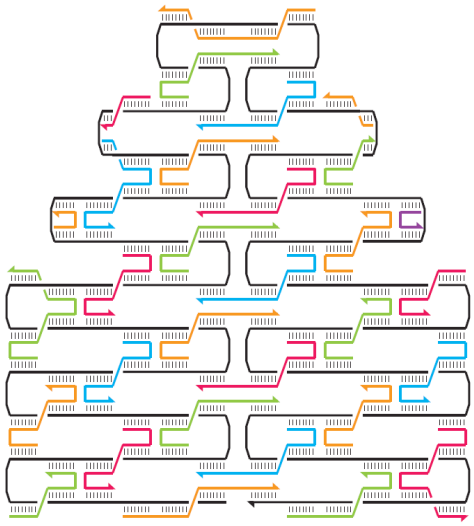

Figure 3: The finished origami with a scaffold strand (black) bonded with crossover and staple strands (red, blue, green)[10]

The basis for the use of DNA in nanotechology is the molecule's ability of self assembly. The Watson-Crick pairing being the favored interaction between the bases of the molecule, it is possible to utilize this complementarity of the bases to design and build a wide variety of geometric shapes. In the case of the DNA origami there are numerous properties which can enable it to be a versatile to be used in various applications. It has been shown that the conductivity of the origami contains both electronic and ionic contribution. This information is significant in the development of future nanoelectronic applications. Single-layered DNA origami structures are limited by their low resistance to mechanical stress. To have a stronger resistance to stress, multi-layered structures have been developed to address this problem, resulting in more rigid 3D arrays of antiparallel helices. Examples of these structures include arrays with hexagonal and rectangular cross-sections. These helices can be twisted by deleting or adding a base pair within the array [17,21].

Besides nanoelectronics, DNA-origamis show great potential for applications in several fields via functionalization. By chemically modifying the surface of the origami it is possible to bind other molecules to it, such as proteins or other nanoparticles [20].

2.3 3D-DNA-origami

The possibilities of DNA nanostructures can be expanded greatly by moving from single-layered origamis to three dimensional structures as mentioned previously. Specifically, a 3D-origami is assembled from a flat array consisting of antiparallel helices that is then folded into a three dimensional honeycomb lattice. The antiparallel scaffold helices are supported by staple strands which are winded around the scaffold in an antiparallel direction thus forming B-form double helices with specific geometrical parameters. The desired shape can be defined from the honeycomb lattice by removing duplex sections and subsequently the remaining duplex sections are connected with a scaffold strand by adding scaffold crossovers at certain positions. To maintain the local crossover density along the helix-helix interfaces crossover staples are added at permitted positions and staple strands are defined by adding nicks into the staple helices. The basic design procedure can be completed by using appropriate computer programs and is depicted in figure 4 [11,20,21].

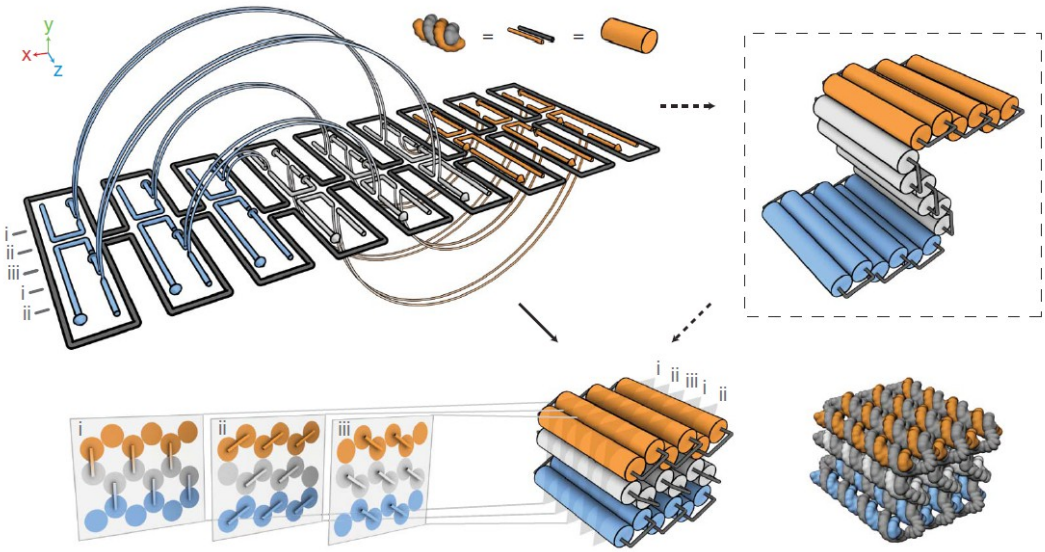

Figure 4: A basic presentation of the formation of 3D-DNA-origamis where the orange, white and blue cylinders are the staple strands held together by crossovers and the scaffold strand (gray)[11]

This approach of using a honeycomb lattice building block as a basis for any desired geometrical shape has been shown to be an effective method for fabricating several different three dimensional structures by Douglas *et al* [11]. Compared to a flat origami there are approximately two times as much crossovers in the honeycomb origami which could be the reason why the inter-helical gaps produced by electrostatic repulsion in the 3D-origami are considerably smaller. The assembly process for 3D-origamis is done similarly to flat origamis where hundreds of staple strands direct the folding via a one-pot reaction with the scaffold strand in a rapid heating and a slow cooling afterwards to achieve the desired shape.

According to Douglas *et al* the presence of divalent cations seem to stimulate the folding rate and conversely monovalent cations appear to have the opposite effect on the folding rate. The effect of the divalent cations can be due to them stabilizing Holliday-junction crossovers (specific) and compact DNA folding intermediates (nonspecific). Monovalent cations could have an antagonizing response due to them possibly competing with the divalent cations. Despite having optimal cation concentrations these nanostructures might require even week-long thermal ramping to achieve the correct folding of the origami. Because of the large density of the crossovers and the confined spaces between the helix layers where the local folding and unfolding takes place the

overall folding of multilayered origamis is not as robust in regards to different annealing conditions compared to more simple origamis [21].

The development of multilayered DNA-origamis could have the potential to broaden the scope of viable applications which might not be achievable with the more traditional flat structures. Similar three-dimensional scaffolding can be found in various molecular machines that are present in living cells, such as ribosomes and polymerases. With this approach to DNA-nanostructures it might not be far-fetched to picture a progression towards comparable synthetic nanomachines.

2.4 Conductivity of DNA

Double stranded DNA (dsDNA) molecules contain overlapping π-orbitals in the base pair stack between adjacent bases. Based on this observation it was concluded in the 1960's that it would be possible for a DNA-molecule to function as an electrical conductor. This subject has been a point of great interest thereafter and the amount of research data obtained concerning it is vast. Initially the results differed greatly from each other with reports ranging from insulating to superconducting behavior. In fact the conductivity is dependent on various parameters such as mismatches or the sequence of the molecule with backbone, nucleotide and ion conductivity contributing to the total net conductivity [12,13].

Possible mechanisms for the conductance include for instance tunneling, thermally induced hopping and already mentioned electronic coupling between orbitals. Orbital coupling, or π-stacking, features the creation of delocalized bonding and antibonding π-orbitals in the aromatic rings of the DNA bases. This can lead to the energy gap between the bonding and antibonding states being severely reduced (semiconductor) or disappearing altogether (ohmic behavior), provided that the electronic coupling between the orbitals of adjacent bases is strong enough. In the case of tunneling a charge is transferred between donors and acceptors in adjacent base pairs by tunneling through the one-dimensional energy-barrier with an exponentially decaying rate depending on the distance between donor and acceptor. Thermal hopping occurs when the charge moves in a diffusion-like manner between intermediate sites. The choice between tunneling and thermal hopping as the mechanism for charge transport is dependent on the number of bases between the donor and acceptor. If it is low, tunneling is dominant (short bridge for tunneling) whereas thermal hopping is preferred when the bridge is long [12,13].

Since the DNA-molecule is fundamentally different from materials with whom terms such as semiconductor or insulator are usually associated, it isn't entirely clear whether it can be described in this manner regarding conductive properties. Instead of a periodic lattice it features a combination of biopolymers with variable charge transport capabilities due to bottlenecks between phase-coherent regions. Due to the large number of such bottlenecks and regions they are largely responsible for the specific transport mechanisms and the electric structure and response in the polymer. The distinction between insulator and semiconductor properties in DNA can be identified by comparing the behavior of the molecule (with a wide band-gap) when a voltage is applied across it. If charge transport can be induced without irreversibly altering the properties and structure of the DNA it can then be classified as a wide bandgap semiconductor. If the applied voltage causes irreversible damage or transformation the molecule is an insulator [13].

According to the so far accumulated information from various measurements there are indeed ways to utilize DNA as a means to transports charge carriers. This can be done all the way from single molecules to networks of bundled molecules, however, the conductivity is not very high. In single, over 40 nm long DNA molecules the charge transport is blocked if the molecule is attached to a surface which might be caused by molecular defects generated by the surface force field. This effect could be weakened by using doped molecules or by reducing the surface affinity of

the molecule to weaken the influence of the surface force field.

In the case of DNA-origamis studies and equivalent circuit analyses indicate that conductivity in these nanostructures is a combination of ionic diffusion and electronic conductivity instead of being solely ohmic. Within the origami the conformation of the constituting DNA-molecules remains relatively stable in proper room conditions and thus many of the conductivity-affecting factors connected to the conformations have reduced effect on the conductivity. According to AC Impedance Spectroscopy (AC-IS) measurements performed on a rectangular DNA-origamis double layer charge transfer and commonly used linker molecules induce high resistances in the molecules and deem DC transport measurement insufficient in providing a complete picture of the conductivity. By using equivalent-circuit models together with the AC-IS measurements the ionic and electronic conductivity contributions can be determined separately, allowing for further applications in the development of nanoelectronic devices based on DNA-origamis [22].

Essentially the measurement of conductivity in a DNA-molecule requires careful consideration as there are numerous variables affecting the result which in turn can lead to conflicting conclusions. The contacts between electrodes and the molecules should be suitably ohmic with low resistances and the environmental factors such as humidity which affects the conformation and conductivity of DNA should be kept in check in order to achieve consistency. Other aspects like counter-ion types, salt concentrations and pH also have their significant part to play as does the type of substrate used and the geometry of the measurement setup (free-hanging DNA or lying on the substrate) [13,22].

2.5 Dielectrophoresis

As opposed to electrophoresis, which refers to the movement of a charged particle in an electric field towards the opposite electric charge, in dielectrophoresis the particle does not need to be charged, just polarizable, and it is moving in a non-uniform electric field [23]. A negative and a positive charge distribution is induced on the opposite sides of the particle by the electric field and a force is induced to both surfaces by the coulombic interaction between the charged surfaces and the electric field [2,14]. The net force difference exerted on the particle due to the inhomogenity of the electric field makes it to move. A simplified presentation of dielectrophoresis is shown in figure 5.

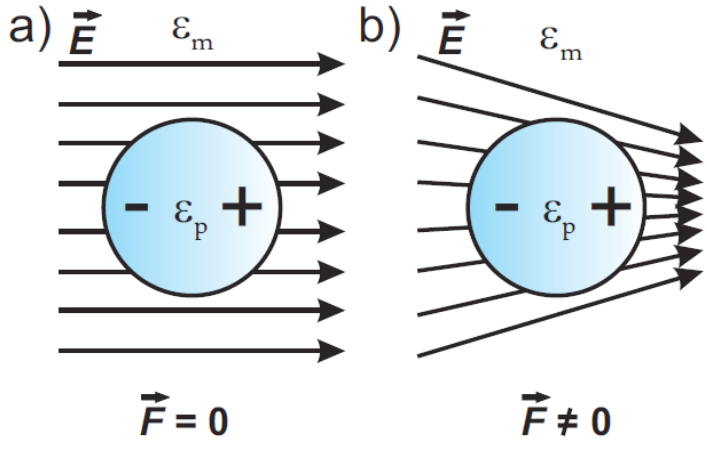

Figure 5: The basic principle of dielectrophoresis [2]

The dipole moment for the dielectric particle and the surrounding medium which can be treated as an effective dipole in electric field is

$$\vec{p} = \alpha \vec{E} \quad , \tag{1}$$

where α is the effective polarizability of the dipole which can be written in a certain direction i as

$$\alpha_i = 3V \epsilon_m \mathrm{Re}(K_i) \quad , \tag{2}$$

where ε_m is the permittivity of the medium, V is the volume of the particle, K is the Clausius-Mossotti factor, which is dependant on both the permittivity of the particle and the medium. Because the field is non-uniform, the net force (dielectrophoretic force) exerted on the particle is not zero and can be defined as

$$\vec{F}_{DEP} = (\vec{p} \cdot \vec{\nabla}) \vec{E} \quad . \tag{3}$$

Because the electric field can be expressed as the negative of the gradient of the potential with $\vec{\nabla} \times \vec{E} = 0$, the above equation can be written with equation (1) as

$$\vec{F}_{DEP} = \frac{\alpha}{2} \vec{\nabla} (E^2) \quad . \tag{4}$$

One can express the time-averaged DEP-force in a periodically alternating electric field $E(t)$ with a period T as

$$\vec{F}_{DEP,t} = \frac{1}{T} \int_0^T \frac{\alpha}{2} \vec{\nabla} [E(t)]^2 dt = \frac{\alpha}{2} \vec{\nabla} \left\{ \frac{1}{T} \int_0^T [E(t)]^2 dt \right\} = \frac{\alpha}{2} \vec{\nabla} (E_{RMS}^2) \quad , \tag{5}$$

where E_{RMS} is the root mean square of the electric field. When combined with equation (2) the time-averaged DEP-force can be written as

$$F_{DEP} = 2\pi \epsilon_m r_p^3 \cdot \mathrm{Re}(K(\omega)) \nabla (E_{RMS}^2) \quad , \tag{6}$$

where r_p is the effective radius of the particle [2]. This net force moves the particle translationally towards either the minimum or the maximum of the electric field, depending on the permittivity of the particle and the medium. Generally when the permittivity of the particle is smaller than that of the medium the particle moves towards the minimum of the electric field (negative DEP) and vice versa (positive DEP). In equation (6) this is represented by the Clausius-Mossotti factor that is

$$K_i = \frac{1}{3} \frac{\epsilon_p^* - \epsilon_m^*}{\epsilon_m^* + N_i (\epsilon_p^* - \epsilon_m^*)} \quad , \tag{7}$$

where N_i is the depolarization factor in the direction i, and $\epsilon^* = \epsilon + \frac{\sigma}{i\omega} = \epsilon - \frac{i\sigma}{\omega}$ is the complex permittivity in which σ is the conductivity and ω is the angular frequency of the electric field. The depolarization factor N_i is dependant on the considered direction and the geometry of the object and it can only be analytically expressed for a particle of ellipsoidal geometry. For the simplest ellipsoidal particle, the sphere, the depolarization factor is N_i = 1/3 for any i and therefore the

Clausius-Mossotti factor simplifies to

$$K(\omega)=\frac{\epsilon_p^*-\epsilon_m^*}{\epsilon_p^*+2\epsilon_m^*} \quad . \tag{8}$$

However, for a an ellipsoid with semi-axes in the three orthogonal directions being a_x, a_y and a_z the depolarization factor in a specific direction can be expressed as

$$N_i=\frac{a_x a_y a_z}{2}\int_0^\infty \frac{ds}{(s+a_i^2)\sqrt{(s+a_x^2)(s+a_y^2)(s+a_z^2)}} \quad , \tag{9}$$

in which s is an integration variable in ellipsoidal coordinates. These depolarization factors for the ellipsoid satisfy the condition

$$N_x+N_Y+N_z=1, \quad N_i\in[0,1] \quad . \tag{10}$$

The solutions for the elliptic integral of equation (9) for a prolate spheroid (ellipsoid of revolution with $a_x>a_y=a_z$) are

$$N_x=\frac{1-e^2}{2e^3}[\ln(\frac{1+e}{1-e})-2e] \quad \text{and} \quad N_y=N_z=\frac{1}{2}(1-N_x) \quad , \tag{11,12}$$

Where e is the eccentricity of the ellipsoid; $e=\sqrt{1-\frac{a_y^2}{a_x^2}}$. Now using equation (2) the effective polarizability for an object can be written as

$$\alpha_i=\epsilon_m V\,\mathrm{Re}[\frac{\tau-1}{1+N_i(\tau-1)}] \quad \text{where} \quad \tau=\frac{\epsilon_p^*}{\epsilon_m^*} \quad . \tag{13}$$

This equation allows the calculation of the depolarization factors and polarizability components of the DNA origami used in the DEP trapping process [2].

Equation (3) signifies that the DEP-force and the gradient of the square of the electric field are parallel and that the direction of the field does not influence the direction of the force in any way. Because the only factor affecting the movement of the particle is the gradient of the applied electric field, dielectrophoresis can also be applied to fields with AC-voltage. The direction of the movement by altering the frequency of the electric field allowing the possibilities for a more intricate control over the particles in a suitable medium. The DEP force being proportional to the volume of the particle may cause inconsistensies when the particles in question are in the nanoscale since the small particles have non-ideal properties that can complicate the process; for example the distribution of atoms in the molecules is not homogenous. Another disturbing factor regarding nanoscale particles is the Brownian motion as it it always present and scales as k_BT/V. This force is significant for nanoparticles since for them $V\to 0$ and therefore it can potentially greatly exceed the DEP force [2,14].

Chapter 3

Methods

3.1 DNA-origami used in this work

The origami structure used for the dielectrophoretic trapping features standard M13mp18 genomic DNA used for a basic 2D-origami shape which was in turn used to form the actual three dimensional structure; a DNA nanotube with an approximate length of 400 nm and height of 2 nm, treated with thiols. A detailed schematic of the structure can be seen below in figure 6.

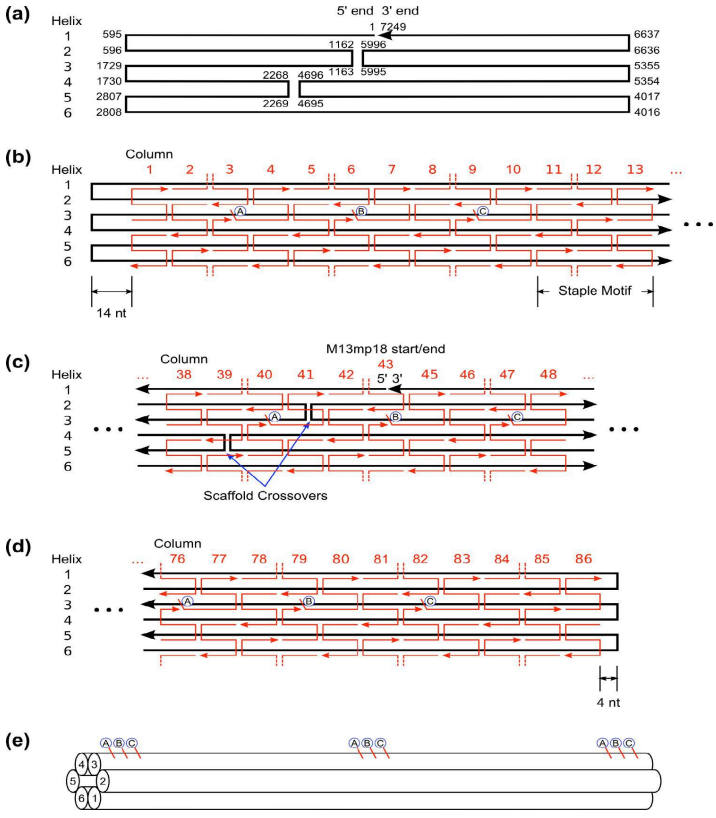

Figure 6: The nanotube structure used in the trapping: a): the scaffold strand that runs through the whole structure in a raster pattern, b): the front section of the structure with staple strands and crossovers added on top of the scaffold, c): the middle section of the structure , showing the scaffold crossovers, d): the end section of the structure, e): the final 3-D shape of the nanotube

3.2 Dielectrophoretic trapping

Dielectrophoresis can be utilized in trapping almost any samples between electrodes by adding a small amount of a solution containing sample particles around the electrodes and applying an electric field between the electrodes. DC-field works for neutral particles but since DNA is negatively charged an AC-field must be used or otherwise all of the particles would flow to the positive electrode. With AC-field this behavior is averaged close to zero. If the permittivity of the sample allows it, the particles will flow towards the maximum of the electric field and take a position between the electrodes because both electrodes would apply an equal force on the particle. However, the movement of the particles is also affected and hindered by the random movement of the molecules and thermal forces applied to them [24,25]. When the sample solution is applied onto the electrodes the charges and molecules present in the solution create flows that can have an opposite direction to the dielectrophoretic movement of the particle. These flows are most commonly caused by thermal convections or AC-electro-osmotic flow. Brownian motion can also prevent the particles from trapping. Brownian motion refers to the random movement of particles in liquids and gases where nanoscale particles are engaged in a constant thermal movement while colliding with other particles. The maximum value of the Brownian random force exerted on a spherical particle can be approximated as

$$F_{Brownian} = \frac{k_B T}{2 r_p} \quad , \tag{14}$$

where k_B is Boltzmann constant, T is temperature and r_p is the radius of the particle. This inverse relation to the radius of the particle leads to smaller particles having a larger random force exerted upon them and therefore they require a larger dielectrophoretic force to move them between the electrodes, although the smaller particles also have a smaller DEP force due to the size dependency. Thus they need larger gradients for a successful trapping. This can also be used to effectively remove unwanted small particles from the gap and leave only the larger, desired particles to be trapped.

Thermal convections are present in the electrode structure since the electric field causes local fluctuations in temperature. It has been shown that the amplitude and frequency of the AC-field as well as the conductivity of the solution all affect the thermal convection. A high frequency (12 MHz) and conductivity (over 300 μS/cm) will direct the flow away from the electrode gap. On the other hand convection flows are always increased by high conductivity. For the origamis this means that a trapping buffer with lower conductivity than the fabrication buffer must be used [25].

The flows can also be generated by AC-electro-osmosis where an electric double layer (EDL) is formed around the electrode surface which is immersed in the liquid [14]. Ions are absorbed into the surface via chemical interactions which in turn attract opposite charges from the liquid, forming the double layer. According to the Stern model [14], the double layer consists of a combination of a diffusion and a solid layer and thus the layer is not wholly solid. Ions can move inside the formed static layer, hence it is referred to as a diffusion layer. Nanostructures have a large ratio of area to volume and systems like this have occurrences of electric double layer. The actual AC-electro-osmotic flow is generated from interactions between the double layer and the electric field. In this case with a gap between two electrodes, a potential is formed between the electrodes by the electric field. The tangent of the field is causing the ions of the double layer to move away from the gap. Since the electrodes have opposing charges the direction is always away from the gap. The electro-osmotic flow is also affected by the thickness of the double layer which is dependant on the concentration and charge of the particles in the solution and thus also dependant on the temperature and conductivity of the solution [25,26].

Dielectrophoretic trapping of the particles can also be described by the DEP potential [2]. As

the negative gradient of the potential energy equals to the force the DEP potential in the electric field can be defined for a uncharged polarizable particle as

$$U_{DEP} = -\frac{1}{2}\alpha E^2 \quad . \tag{15}$$

The total potential energy for the particle can be obtained by combining the DEP potential with the thermal energy of the particle which corresponds to the Brownian motion of the particle:

$$U_{total} = U_{DEP} + U_{thermal} = -\frac{1}{2}\alpha E^2 + \frac{3}{2}k_B T = \frac{3}{2}k_B - \frac{1}{2}\alpha E^2 T \quad . \tag{16}$$

This is valid for neutral particles since the formula does not consider electrophoretic effects, but also for non-neutral particles that are in an AC-field as the time-average of electrophoretic forces is zero for such particles. Considering the trapping, this signifies that there is a DEP potential well, located at a position where the absolute value of U_{DEP} is equal or higher than $U_{thermal}$.The dielectrophoretic force pushes the particles towards the bottom of the potential well which is the minimum of the total potential energy [2].

3.3 Effective polarizability of the DNA-origami

In order to calculate the individual components for the effective polarizability, one must first find out the values for the corresponding depolarization factors [2,27]. It is assumed that the thickness of the counter-ion cloud surrounding the origami structure is approximately 20 nm [2], this being the value in conditions which are similar to the ones used in the trapping. Since the origami itself has a length of 400 nm and height of 5-6 nm, the semi-axes for the corresponding ellipsoid (prolate) are a_x = 210 nm and $a_y = a_z$ =13 nm. Now from equations (11) and (12) the depolarization factors can be calculated as $N_x \approx 0.0095$ and $N_y = N_z \approx 0.50$.

To obtain the polarizability components for the origami with the depolarization factors a few simplifications have been made [2]. The medium solution is treated as water and therefore $\epsilon_m = \epsilon_{water} \approx 7.1 \cdot 10^{-10}$ F/m . Additionally, the permittivity value for the DNA and the ion cloud surrounding it is approximated as $\epsilon_p \approx 2.6 \cdot 10^{-9}$ F/m [2]. This value has been calculated by using a 444 bp long dsDNA molecule immersed in a solution (with approximate polarizability of $8 \cdot 10^{-32}\,\mathrm{Fm}^2$) as a reference molecule. Using these estimations one can obtain a simplified formula for the polarizability components:

$$\alpha_i \approx \frac{\epsilon_{water} V}{0.38 + N_i} \quad . \tag{17}$$

By substituting the depolarization factors calculated above and the volume of the ellipsoid in the equation above one obtains the effective polarizability components for the 3D-DNA origami:

$$\begin{cases} \alpha_x \approx 1.94 \cdot 10^{-31}\,\mathrm{Fm}^2 \\ \alpha_y = \alpha_z \approx 8.63 \cdot 10^{-32}\,\mathrm{Fm}^2 . \end{cases}$$

It can be seen from the results above that the effective polarizabilities of the origami depend strongly on the direction, as the polarizability component in the *x* direction is significantly larger when compared to the components in *y* and *z* directions [2].

3.4 Dielectrophoretic force in the electrodes

To find out how the dielectrophoretic force behaves around the gap in the electrode structure used in the experiments a series of simulations were done in order to illustrate this aspect of the trapping. These simulations were done with COMSOL Multiphysics 4.4 software.

The model features the basic geometry of the 20 nm high gold fingertip electrodes on a SiO_2 surface with the buffer solution covering the electrodes. The buffer is treated as being water with relative permittivity of 80. Since the dielectrophoretic force is directly proportional to the gradient of the square of the electric field according to equation (6), the force was simulated with this gradient to represent it graphically.

Simulations were done for both of the electrode geometries (150 nm and 400 nm gap) with DC voltages corresponding to the rms-values of the AC voltages used in the experiments (1 V, 1.2 V, 1.5 V). The tips of the electrodes were rounded in order to produce a more realistic representation of the fabricated electrodes. The results for the simulations are presented in figure 7.

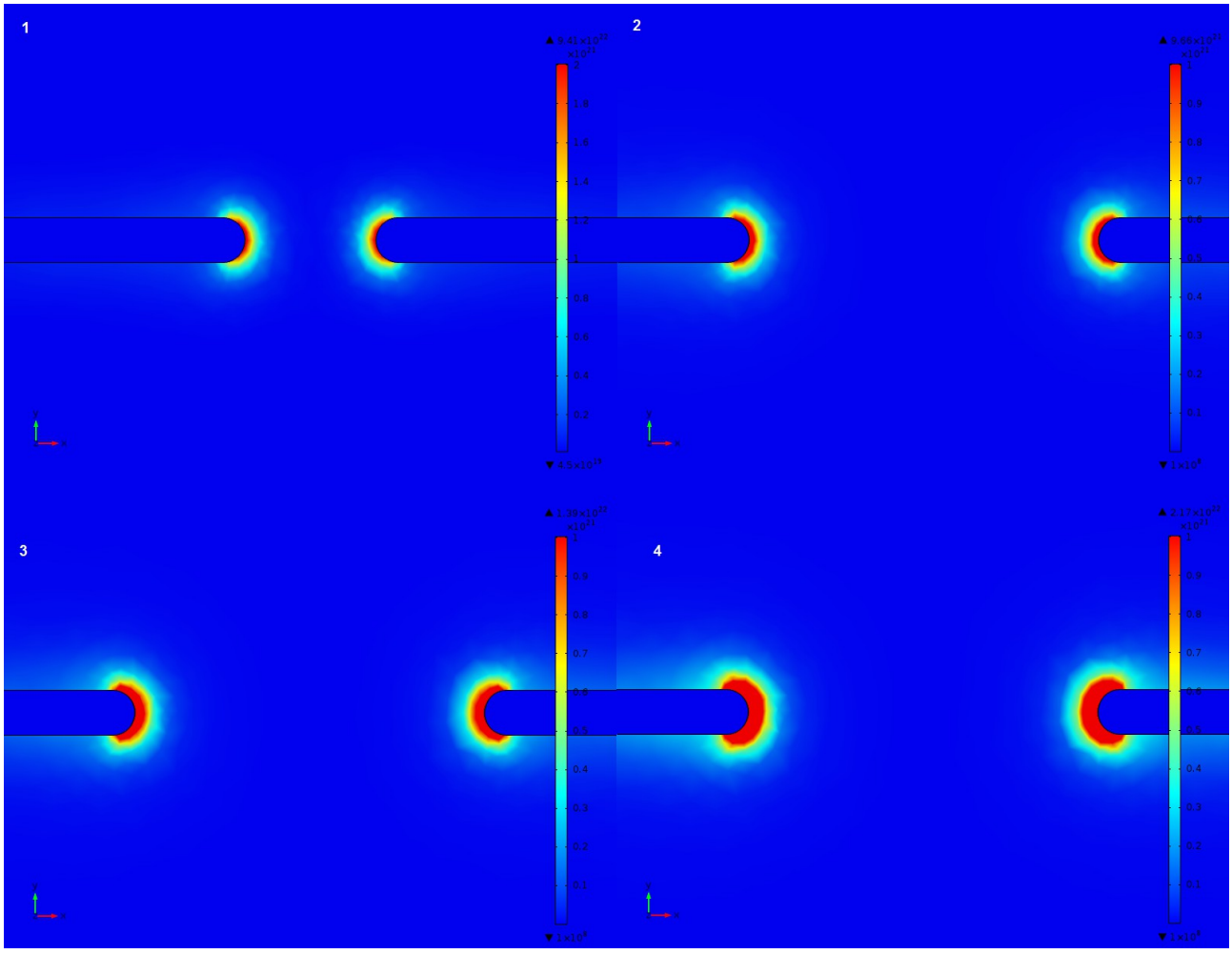

Figure 7: Simulation of the gradient of the square of the electric field corresponding to the dielectrophoretic force with 150 nm gapsize and voltage of 1 V (1) and 400 nm gapsize and voltages of 1 V, 1.2 V and 1.5 V (2, 3 and 4 respectively)

As can be seen from figure 7, the gap size does not seem to have much of an effect on the DEP force whereas the area of the maximum force steadily grows with larger voltages. The maxima of the force and electric field are located at the tips of the electrodes whilst having significantly weaker presence along the rest of the electrodes. The simulations provide a clear demonstration for the theoretical basis of dielectrophoresis.

Now from figure 7 one can obtain the maximum value for the gradient of the square of the electric field. Using this value and the *x* direction polarizability component one can calculate the maximum DEP-force exerted on the origamis for each of the cases presented in figure 7 and compare it to the Brownian random force:

$$\vec{F}_{DEP\,150\mathrm{nm}\,1\mathrm{V}} = \frac{\alpha_x}{2}\vec{\nabla}(E^2) = \frac{1.939968\cdot 10^{-31}\,\mathrm{Fm}^2}{2}\cdot 9.41\cdot 10^{22}\frac{\mathrm{V}^2}{\mathrm{m}^3} = 9.127549\cdot 10^{-9}\,\mathrm{N} \approx 9.13\cdot 10^{-9}\,\mathrm{N}$$

$$\vec{F}_{DEP\,400\mathrm{nm}\,1\mathrm{V}} = \frac{\alpha_x}{2}\vec{\nabla}(E^2) = \frac{1.939968\cdot 10^{-31}\,\mathrm{Fm}^2}{2}\cdot 9.66\cdot 10^{21}\frac{\mathrm{V}^2}{\mathrm{m}^3} = 9.370045\cdot 10^{-10}\,\mathrm{N} \approx 9.37\cdot 10^{-10}\,\mathrm{N}$$

$$\vec{F}_{DEP\,400\mathrm{nm}\,1.2\mathrm{V}} = \frac{\alpha_x}{2}\vec{\nabla}(E^2) = \frac{1.939968\cdot 10^{-31}\,\mathrm{Fm}^2}{2}\cdot 1.39\cdot 10^{22}\frac{\mathrm{V}^2}{\mathrm{m}^3} = 1.3448277\cdot 10^{-9}\,\mathrm{N} \approx 1.35\cdot 10^{-9}\,\mathrm{N}$$

$$\vec{F}_{DEP\,400\mathrm{nm}\,1.5\mathrm{V}} = \frac{\alpha_x}{2}\vec{\nabla}(E^2) = \frac{1.939968\cdot 10^{-31}\,\mathrm{Fm}^2}{2}\cdot 2.17\cdot 10^{22}\frac{\mathrm{V}^2}{\mathrm{m}^3} = 2.104865\cdot 10^{-9}\,\mathrm{N} \approx 2.10\cdot 10^{-9}\,\mathrm{N}$$

$$F_{Brownian} = \frac{k_B T}{2 r_p} = \frac{1.3806488\cdot 10^{-23}\frac{\mathrm{m}^2\,\mathrm{kg}}{\mathrm{s}^2\,\mathrm{K}}\cdot 293\,\mathrm{K}}{2\cdot 200\,\mathrm{m}^{-9}} = 1.01132525\cdot 10^{-14}\,\mathrm{N} \approx 1.01\cdot 10^{-14}\,\mathrm{N}.$$

Trapping particles is possible if the applied DEP force is greater than the random force exerted on the particles. Now this condition is satisfied in all cases above as the DEP force is significantly larger than the Brownian force. Similar result is also obtained when *y/z* direction components are used for the calculation.

3.5 Atomic force microscope

Atomic force microscope (AFM) functions by probing the surface of a sample with a nanometer scale silicon tip attached to a flexible cantilever. Interactions between the surface and the tip cause deflection and these vertical and horizontal movements of the tip are measured with a laser that is reflected from the cantilever into a photodetector. The force and the distance between the tip and the sample surface is kept constant by modifying the vertical position of the tip and the cantilever and these alterations provide the information from which an image of the sample surface is constructed [28,29].

The cantilever bends in a specific way when it is interacted upon by a perpendicular force. These deviations are measured by using a beam deflect method where the reflected laser beam is aimed at the center of a four-field photodetector. As the beam hits the detector a voltage signal is produced unless the cantilever is not bent and the beam is at the center of the detector. When the cantilever bends the position of the reflected beam changes on the detector which enables the measurement of the movements of the cantilever through the changes in the signal produced by the

photodetector [28,29].

The signal obtained from the tip is run to a feedback loop which is shown in figure 8. The error signal obtained from the feedback loop indicates the amount that the tip position needs to be adjusted in order to keep the force between the tip and the sample constant. The error signal is amplified and modified and fed into a piezoelement that will adjust the z-movement of the tip. For DNA and other soft materials it is best to run the AFM in tapping mode where the tip oscillates near its resonance frequency, only slightly touching the sample in the lowest point the oscillation. In this mode the feedback loop signal tells how the tip needs to be lowered or raised so that the amplitude will approach a specific set-point. In contact mode the tip is in contact with the sample and accurately follows the surface due to repulsive van der Waals forces, giving good resolution but potentially damaging the sample and the tip [30].

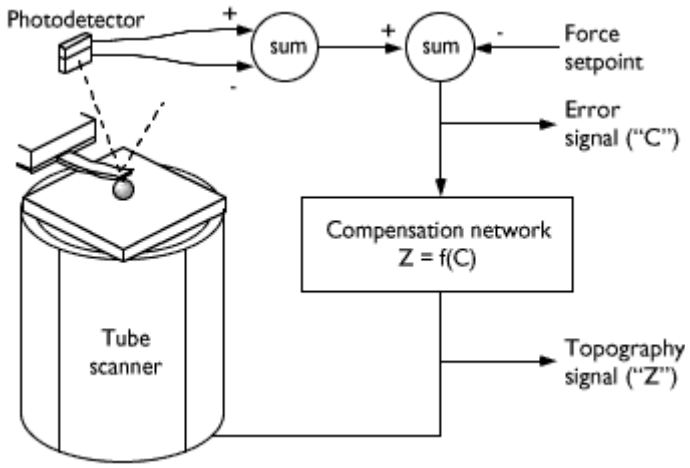

Figure 8: The feedback loop of the AFM [31]

In order to accurately alter the position of the cantilever and the tip piezoelements are utilized. These elements consist of specifically shaped piezoelectric material with attached electrodes. When affected by an electric field the elements either decrease or increase in size depending on the voltage because of the anisotropicity of the crystalline structure. The most common piezoelectric material used in atomic force microscopes and other such instruments is lead zirconate titanate which is used for its relatively high Curie temperature (200-400 ^{o}C) that signifies the threshold above which the piezoelectric behavior disappears [29,30].

The most simple method for positioning the tip is to have an individual piezoelement for each of the x-, y- and z-coordinates. With this configuration the x- and y-elements move sample and the z-element moves the tip. Another option is to use a tube scanner that moves either the tip or the sample. The scanner moves in z-direction by increasing or decreasing in size axially due to the voltage from the outer wall electrodes. X- and y-movements is done by bending the tube with oppositely charged voltages that come from opposite electrodes. The AFM has a long imaging time that is caused by the piezoelements having a slow response time as the tip requires constant adjusting according to the geography of the sample surface. These adjustments are made with a certain frequency which is significantly smaller that the mechanical undamped frequency of the scanner which is in the range of 10 kHz. Due to this the scanning speed is essentially limited to below 100 μm/s [29,30].

3.6 Fabrication methods used

3.6.1 The electrode structure

Two slightly different fingertip electrode types were used for the dielectrophoretic trapping of the origamis. The first set of trapping was done with electrodes that had a gap size of 150 nm whereas the second set featured electrodes with a gap size of 400 nm. The electrodes were fabricated by utilizing electron beam lithography and physical vapor deposition.

3.6.2 Spin coating

To prepare for the lithography the SiO_2 surface must first be coated with a thin film of specific material (resist) on which the lithography pattern is produced. The material depends on the lithography method but the solution usually contains polymers and in the case of electron beam lithography poly(methyl methacrylate) (PMMA) is used. A droplet of the resist material is pipetted onto the surface of the sample which is then rotated at a high speed for a certain amount of time to to spread the resist over the sample surface with centrifugal force. This results in a nanoscale thin film, the thickness of which can be adjusted by modifying the spinning parameters [32].

After the deposition of the resist the sample is heated for a set amount of time (baked) in order to achieve a solid film via polymerization of the resin and to remove any remaining solvent that could still be present in the film from the resist solution. As mentioned above, the significance of the resist material layer is to act as a medium on which the lithography pattern will be transferred during the fabrication process [32].

3.6.3 Electron beam lithography

As the name suggests, electron beam lithography refers to the use of an electron beam, as opposed to photolithography, in order to produce custom designed patterns in a very small resolution. For this purpose a modified scanning electron microscope (SEM) is used for the patterning. The SEM has three main components: an electron gun which produces the beam of electrons, a series of electromagnetic lenses that are required for the focusing of the electron beam and for the scanning of the sample surface, and a set of detectors that are needed for the measurement of the electron scattering from the sample. The SEM requires a vacuum to be formed inside the sample chamber as the electrons would otherwise scatter already from the ambient gas present [32,33].

Resolution of an SEM varies between 1 nm and 20 nm depending on the instrument used. Due to the utilization of the electron beam samples that require imaging need to be electrically conductive which means that samples that do not naturally have conducting properties need to be coated with an ultrathin layer of a conducting material, for example gold. Not having a conducting sample would produce image artifacts due to the electron beam causing charging in the sample. Also because the SEM functions with a vacuum, the samples must be completely dry for this purpose. Thus biological samples need to be chemically fixated to preserve the stability of their structure before using the SEM [33].

For imaging with the SEM there are three different methods. The first one is using the backscattered electron detector, which detects the high-energy incident electrons which have scattered elastically from the sample. The second one uses the secondary electron detector which sense the lower-energy electrons that are driven away from the sample in inelastic scatterings. They

carry more information about the sample surface because they escape from the sample only from a small volume close to the surface. The third detection option is the energy-dispersive X-ray spectroscopy (EDX) which is used for elemental analysis of the sample. Different elements can be identified by the X-rays (with different energies) emitted by the sample when a higher-energy electrons fill the vacancy left in the electron structure by the scattered secondary electrons. The software provides a spectrum where different elements in the sample are displayed. EDX cannot however detect elements whose atomic number is less than four, namely H, He and Li [33].

In lithography a computer is used to guide the electron beam to sweep across the sample surface and draw out a desired pattern. This it inflicts changes in the resist material on the exposed regions of the sample. The exposure initiates a photochemical process in the resist where the polymer chains of the material either break (positive resist) or crosslink with each other (negative resist) in the area of exposure. When the chains break the material becomes more soluble whereas crosslinking prevents solubility. This enables for the resist material to be removed either from the exposed or unexposed areas with a suitable solvent depending on the type of resist used (development). The patterns fabricated this way can be under 10 nm in resolution [32,33]. The PMMA used in this work is a positive resist.

The electrostatic lenses present in the SEM are used for the movement and controlling of the electron beam during the exposure, although in the case of larger patterns the sample stage itself is moved instead of the beam. The pattern being exposed is divided into several separate working areas which have different sizes and are exposed in succession. A significant factor in obtaining a sharp pattern is to adjust the electron beam to have a correct focus. This can be done by exposing a contamination dot on the sample away from the planned pattern area and then adjusting the focus until a sharp dot is acquired. The amount of time required for the exposure of a certain area can be obtained from equation

$$T = \frac{D \cdot A}{I} \quad , \tag{18}$$

where D is the dose of the charge over an area needed, A is the exposed area and I is the beam current. For samples that require relatively large areas to be exposed the exposure time can get quite long and therefore electron beam lithography is not the most suitable method for larger scale microfabrication [33]. In this case usually photolithography is used instead.

3.6.4 Reactive ion etching

Reactive ion etching (RIE) is a dry etching method where plasma-enhanced chemical reactions are utilized to etch solid material away from a wafer providing the process with good selectivity. The etching is done by placing the sample on an electrode that is capacitively coupled to a radio frequency (RF) source. A vacuum is created within the chamber and suitable reactive gases are excited with the RF-plasma. The excitation generates excited and ionized species of which the excited species are very reactive whereas the ionized species create the necessary ion bombardment that is needed to bring energy to the sample surface. This etching process can be completed at a room temperature [32].

The reactive gases that are used for the etching are chosen based on the volatility of the reaction product. A product with a low volatility (low vapor pressure) is harder to pump away from the reaction chamber. RIE has a minimal lateral etching speed and therefore anisotropic etching equals vertical etching in this method. The anisotropicity can be increased with an increased ion bombardment via higher RF power or lower pressure leading to higher mean free path. Inert gases acting as stabilizing agents can be used in the process for enhancing the ion bombardment [32].

3.6.5 Ultra-high vacuum evaporation

After the lithography and development is done and the residual PMMA has been etched away from the pattern with RIE a thin metal film is deposited onto the sample surface to fill the pattern forming the final electrode structure. The deposition is done by evaporating metal with a well-focused electron beam in an ultra-high vacuum (UHV) evaporator. The focusing of the beam is done to have localized heating in the metal and to not yield any contamination since the crucible holding the metal will stay cold without any chemical reactions occurring during the evaporation. The evaporated metal particles travel to the sample ballistically without any collisions because of the vacuum and will therefore only cover an area that is "visible" from the point from which metal is evaporated [32].

Diffusion is prevented on the substrate (sample) by the ballistic transport and high temperature difference between the materials which causes the particles to stuck to the first position they hit on the surface in most cases. Thus the thin film is amorphous and has no crystalline structure as it quickly solidifies on the substrate due to lower temperature. The evaporator features a shutter shield to prevent the evaporated metal from getting to the sample when the evaporation speed is being stabilized. The target material to be evaporated should have a high enough vapour pressure to ease the evaporation, usually higher than surrounding pressure (the vapour pressure of the material should be usually higher than 10^{-2} mbar). These properties also ease the ballistic transport of the particles, lowering the contamination of the chamber since in high or ultra high vacuum the mean free path of particles is mostly larger than the diameter of the vacuum chamber itself. An ultra-high vacuum means that the pressure of the chamber is lower than 10^{-7} mbar as opposed to high vacuum (10^{-3}-10^{-7} mbar) [32].

To achieve the desired thickness of the thin film a Quartz Crystal Microbalance (QCM) is used to monitor the thickness of the deposited layer. The QCM has a very precise resonance frequency which is highly sensitive to changes in mass and can thus detect exceedingly minute changes (even 100 times smaller than precision scales) [32].

3.7 The fabrication process

The fabrication process for the electrode sample is initialized by cutting a 7x7 mm^2 piece from a silicon wafer coated with silicon dioxide (SiO_2). This chip is then cleaned by immersing it in hot acetone after which it is immersed in isopropyl alcohol (IPA) and sonicated for 1-2 minutes. After sonication the chip is thoroughly cleaned with a cotton stick, washed with IPA and dried with N_2.

After preparing the chip a 100 nm film of PMMA was deposited using spin coating with BIDTEC SB100 spinner and 950 PMMA A2 resist. The spinning was done at 2000 rpm for 60 s and the chip was then baked for five minutes at 160 ºC on a hot plate. After depositing the resist the chip was attached to the sample stage of the SEM (Raith eLine) and transferred into the exposure chamber. The dimensions of the sample were measured to ensure that the pattern would be at the center of the chip. The electron beam was focused by using contamination dots to see the size and shape of the focused beam. After focusing the actual patterning process was initialized. The exposure was done in three phases; first the sharp ends of the electrodes were drawn with the gap between them, then the rest of the electrodes were drawn with the large pads on the opposite ends of structure being the final layer. Therefore, the whole pattern uses three working areas whose sizes from smallest to largest were: 10 µm, 200 µm and 2000 µm which correspond to the three separately exposed areas of the electrode mentioned previously.

After exposure the sample was developed by immersing it in MIBK (methyl isobutyl ketone) developer solution for 30 s and then in IPA for 30s and drying it with N_2. The samples were also inspected with an optical microscope to see any anomalies in the pattern which might have

been caused for example by improperly focused electron beam in the SEM. The development was followed by RIE treatment which was used to remove any remaining PMMA residue that might still be present in the pattern. A 10 second O_2 etch was used for this purpose with RF power of 15 W and oxygen flow of 50 sccm. Once the etching was complete the UHV evaporator was utilized to deposit a 2 nm thick titanium film on the pattern. On top of the titanium a 15 nm layer of gold was deposited. Titanium was used to enhance the adhesion of the gold layer. The fabrication was finalized by immersing the samples in hot acetone and leaving them for lift-off overnight. Any leftover resist and metal was then removed via cleaning and sonication and a final cleaning was done by running a one minute O_2 plasma etch in the RIE with 25 W RF power and 50 sccm oxygen flow.

Chapter 4

Experiments and results

4.1 Dielectrophoretic trapping

Before the trapping was initiated the samples were filtered through centrifugal filter units to remove any impurities and to change the high ionic content fabrication buffer to a low conductivity trapping buffer. The filtered solution contained 10 µl of the original origami sample and 490 µl of Hepes/MgAc trapping buffer. This solution was centrifuged at 15800 relative centrifugal force (rcf) for three minutes after which 460 µl of trapping buffer was added to replace the already filtered buffer and the sample was centrifuged for additional five minutes at 15800 rcf. The purified origami solution was collected by centrifuging the filter upside down for another two minutes at 320 rcf. The trapping buffer is required as it has a conductivity of approximately 300 µS/cm which will enable the successful DEP during the trapping.

The DEP trapping of the origamis was carried out by first attaching the electrode structure to the grounded trapping stage. A grounding bracelet was used at all times to prevent static electricity from destroying the sample. The trapping stage was then placed inside a metal box with coaxial outputs. A small amount of water was added into this trapping chamber to prevent drying. The trapping stage was connected to an AC-source and 5 µl of the filtered origami solution, diluted with the trapping buffer, was pipetted on top of the electrode. A sinusoidal AC voltage was applied to the sample for 3 to 5 minutes. The frequency was varied between 10 MHz and 15 MHz while the voltage was 1 V, 1.5 V or 1.2 V depending on the experiment. 1/10, 1/14 and 1/5 dilutions were used for the origami solution. After the voltage was turned off the sample was rinsed with distilled water and dried with a nitrogen flow.

4.2 Imaging

4.2.1 Origami characterization

After the DEP-trapping each sample was imaged with AFM (*Digital Instruments Dimension 3100*, Nanoscope IV). Among other things the images taken demonstrate that the origamis kept their structure intact during the trapping and consequent washing and drying process. In figures 9-19 the imaged results of the DEP-trapping are presented for samples with various trapping parameters.

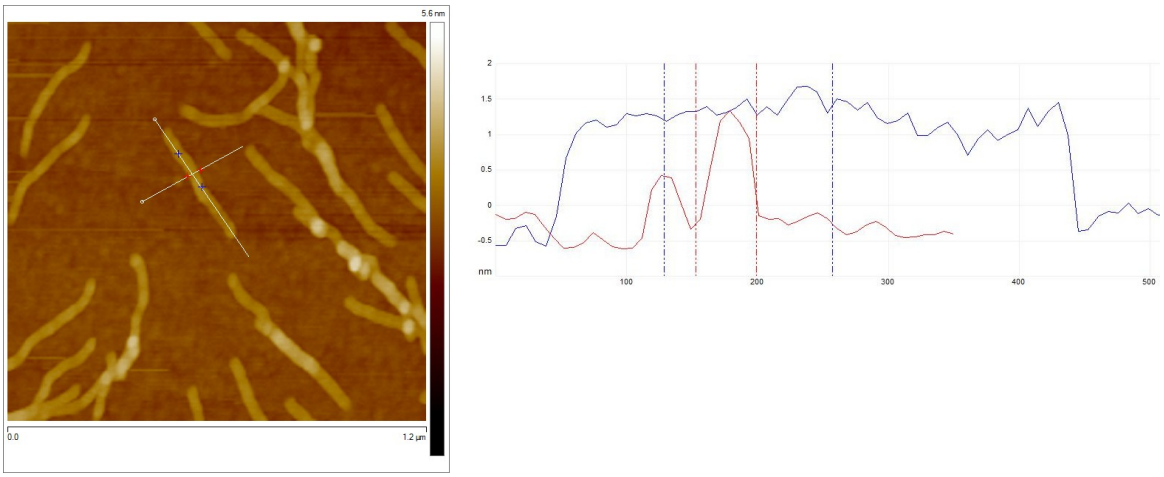

Figure 9: The dimensions of the DNA origamis

In figure 9 one can see details of the origamis that were used for this work. The sample was made by depositing 5 µl of origami solution on mica and letting it settle for 5 minutes. After this the sample was washed three times with 50 µl of water and dried with N_2. As the measurements show all of the nanostructures had an approximate length of 400 nm and height of 2 nm. The actual height of the origamis is more likely to be 5-6 nm since they tend to be collapsed in AFM images. These values were used for the calculation of the polarizability components earlier. Additionally in most cases the origamis seemed to be rather thick horizontally but whether this is due to some kind of collapsing of the nanotubes or just inaccuracy produced by the width of the tip in AFM measurement is not certain.

4.2.2 Trappings with 150 nm gap electrodes

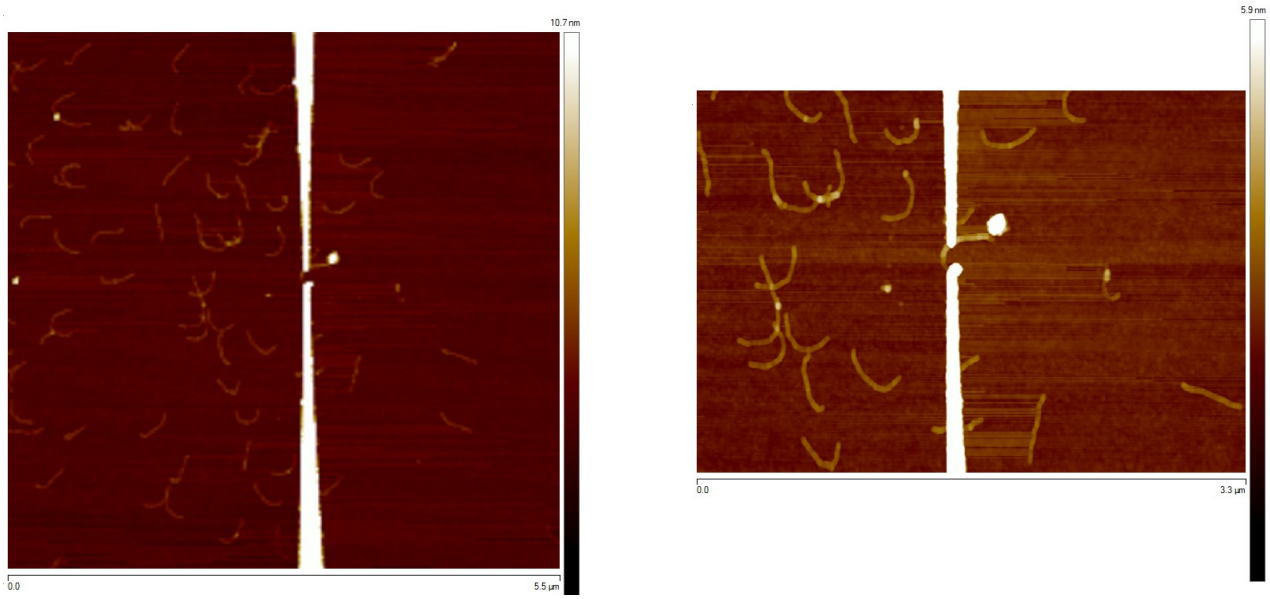

Figure 10: A succesfully trapped origami from batch 20140716 with 1/10 dilution, 1.0 V trapping voltage, 10 MHz trapping frequency and 3 min trapping time with a zoomed-in image of the gap area on the right

In figure 10 is presented a successful trapping of a single origami between electrodes with a 150 nm

gap. Because the origami itself has a length of 400 nm, it extends beyond the electrodes. Curiously, most of the visible origamis have bent themselves in a similar fashion. Also it is evident how majority of the origamis are concentrated on one side of the electrodes which suggests that during the trapping there has been some kind of flow in that particular direction.

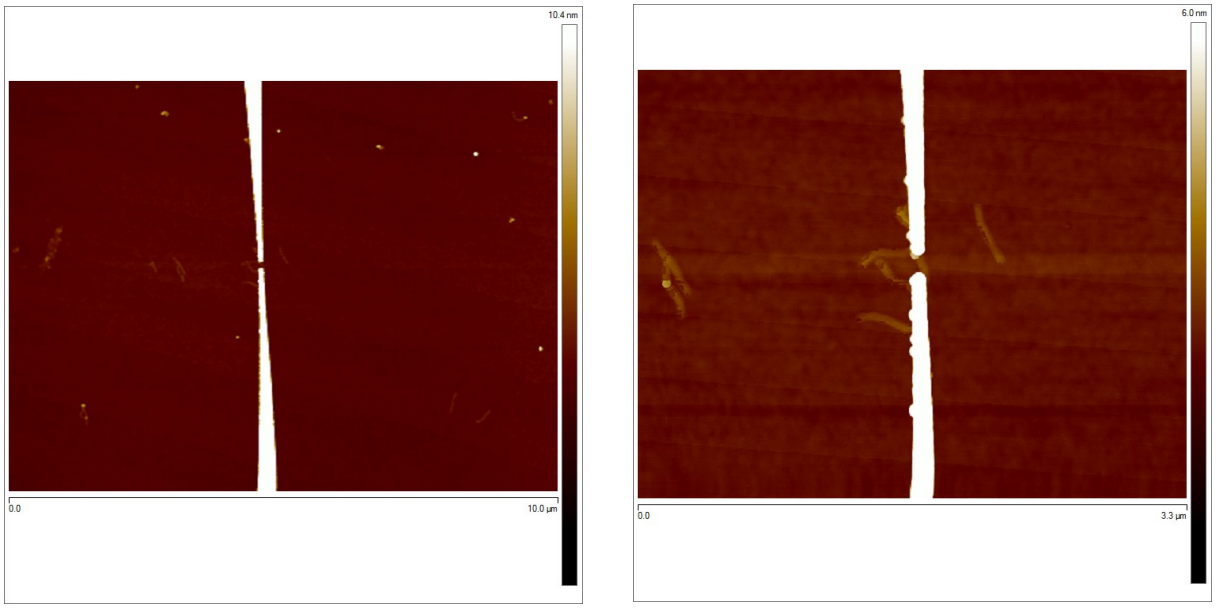

Figure 11: Successfully trapped origamis from batch 20140717 with 1/14 dilution, 1.0 V trapping voltage, 15 MHz trapping frequency and 3 min trapping time with a zoomed-in image of the gap area on the right

Figure 11 shows a successful trapping with a 150 nm gap electrode. According to length measurements, there are two separate ~400 nm origamis attached to each other and trapped between the electrodes. Due to the lower origami concentration of the solution used for this trapping the sample does not feature as much additional origamis as for example the previous one in figure 9 where a higher concentration solution was used.

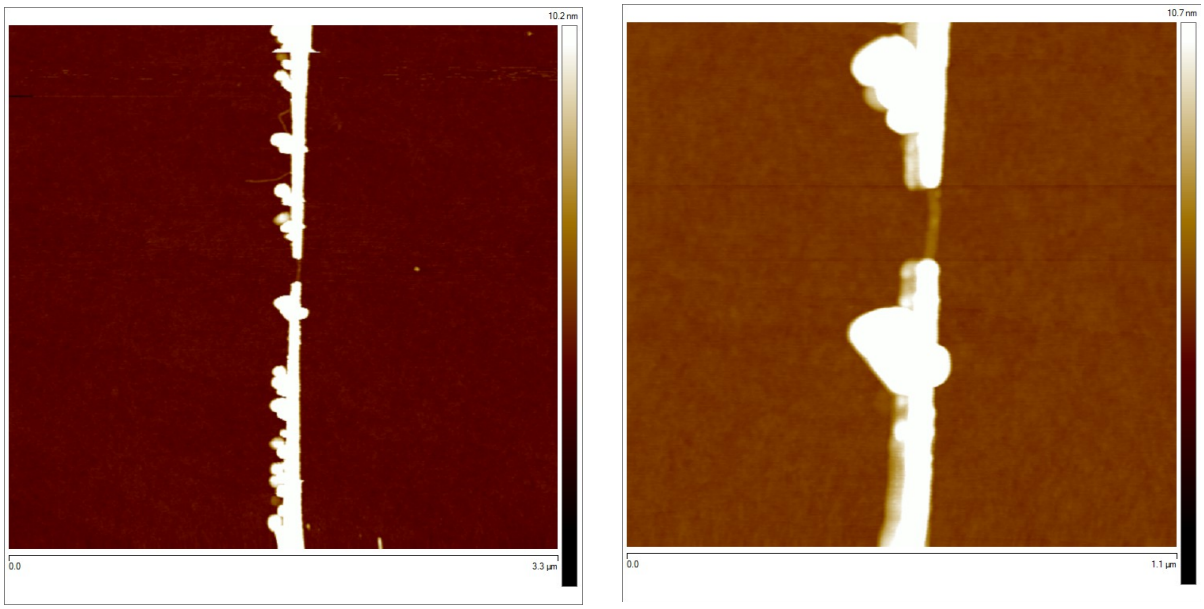

Figure 12: A successfully trapped origami from batch 20140718 with 1/14 dilution, 1.0 V trapping voltage, 15 MHz trapping frequency and 5 min trapping time

Despite the rather large amount of impurities and double-tip behavior during the AFM imaging figure 12 still features a particularly distinct trapping of a single origami with only few additional origamis attached to the electrode structure. Similarly to the previous sample this one also was made using a lower origami concentration solution.

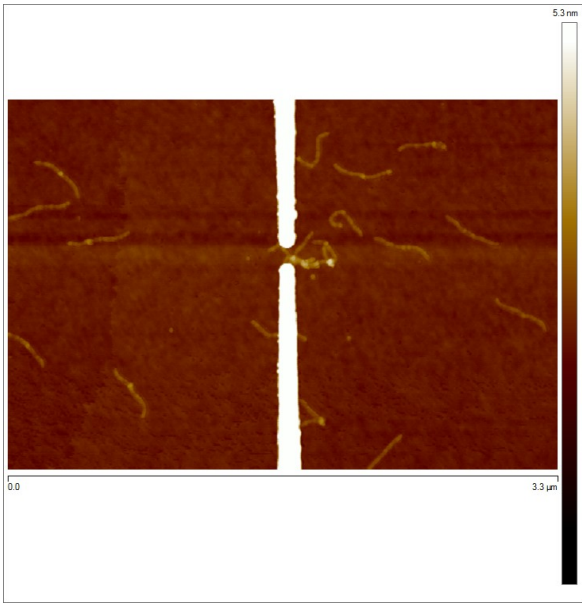

Figure 13: Successfully trapped origamis from batch 20140731 with 1/14 dilution, 1.0 V trapping voltage, 10 MHz trapping frequency and 5 min trapping time

Figure 13 shows a multitude of origamis present within the electrode gap along with some additional particles. Compared to the earlier samples which were also done with the 1/14-diluted origami solution, the large number of origamis is quite deviating. This could be caused by the fact that this trapping was done with a lower trapping frequency (10 Mhz) than the earlier samples (15 Mhz).

4.2.3 Trappings with 400 nm gap electrodes

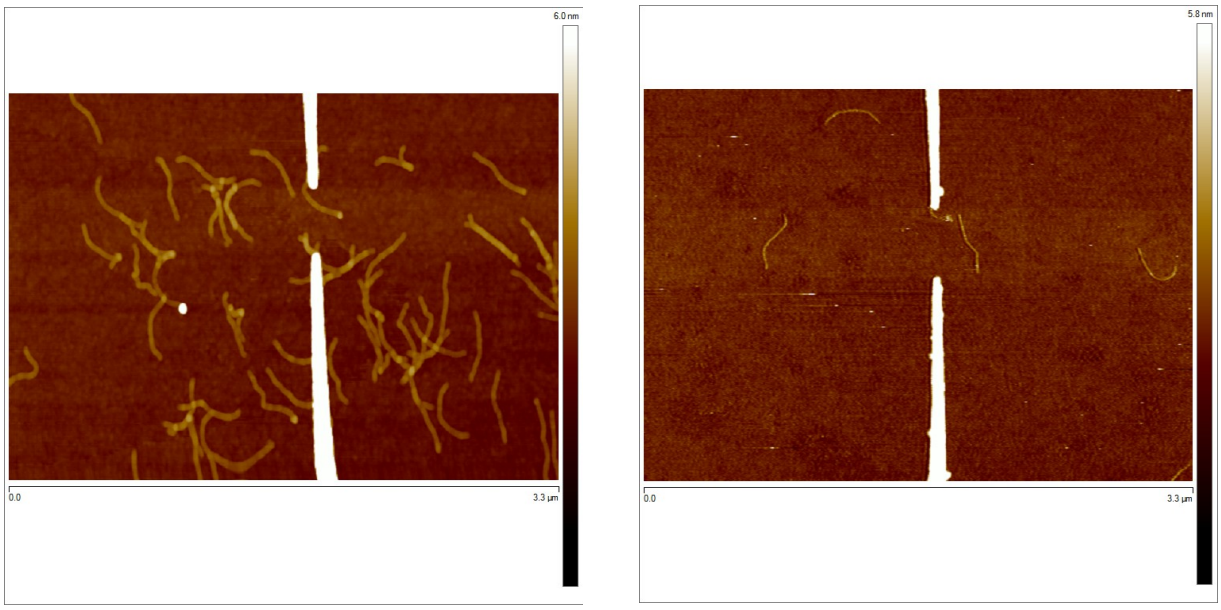

Figure 14: Two samples form batches 20141111 and 20141117 with 1/10 dilution, 1.2 V trapping voltage, 15 MHz trapping frequency and 3 min trapping time

Figure 14 has two samples made with the exact same parameters using electrodes with a 400 nm gap. Though the trapping itself was not successful with these samples, they still show that even the same sample trapping parameters can produce significantly varied results at least in terms of number of origamis. Most probably this is a product of the fact that even the tiniest factors can affect the outcome of the experiment owing to the properties of DNA.

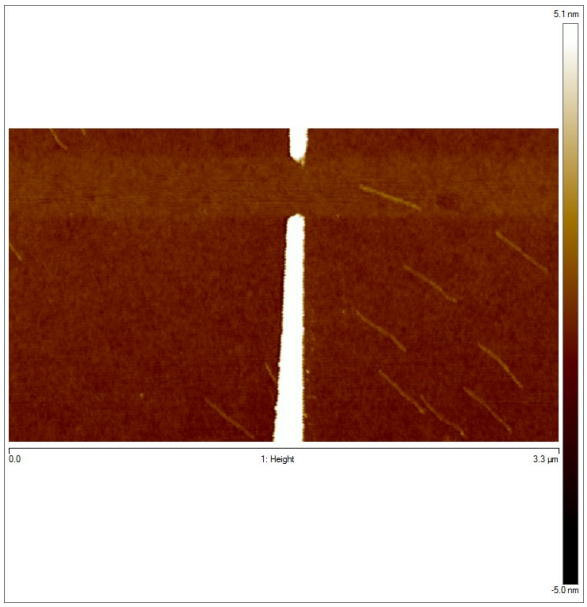

Figure 15: A sample from batch 20141126 with 1/10 dilution, 1.2 V trapping voltage, 15 MHz trapping frequency and 3 min trapping time

Figure 15 shows another unsuccessful trapping with the 400 nm gap electrode, but it has an interesting aspect in that it shows the origamis oriented roughly parallel towards the gap of the electrode. This is evidence that there has been a flow in this sample away from from the gap.

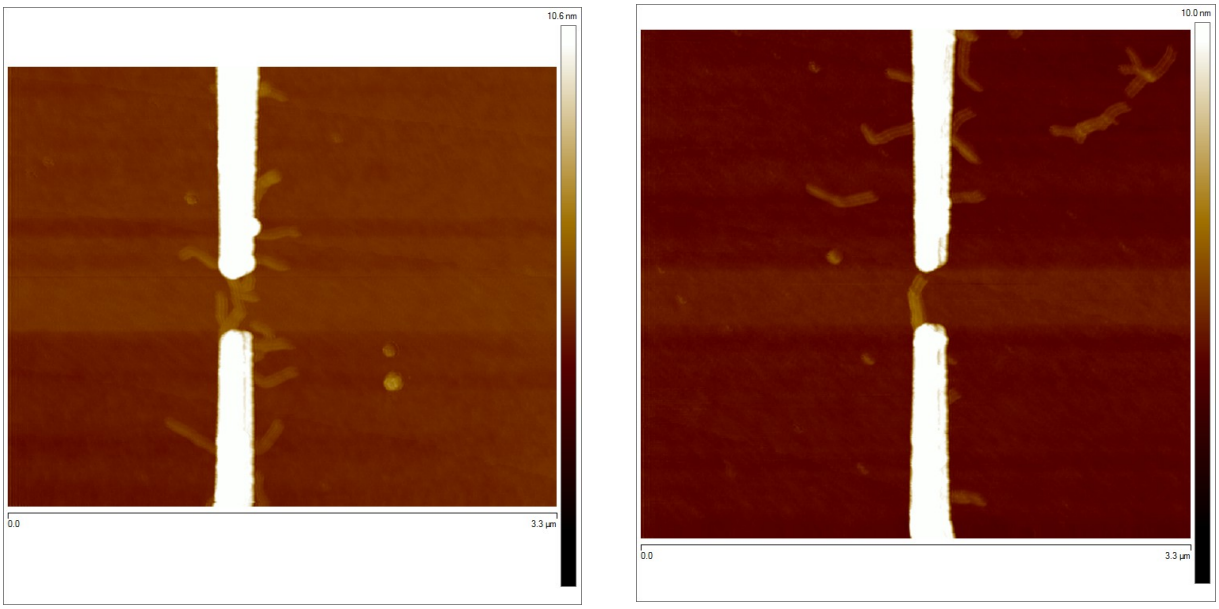

Figure 16: Successfully trapped origamis from batch 20141028 with 1/10 dilution, 1.2 V trapping voltage, 15 MHz trapping frequency and 3 min trapping time

The only successful trappings concluded with the 400 nm gap electrodes can be seen in figure 16 (with triple-tip effect during the AFM imaging). Because of the sudden success with these two samples, most of the following experiments were done with the same parameters in an attempt to replicate the results and to produce a set of nicely trapped origamis with these settings. However, this was not successful and overall this electrode with a larger gap proved to be very challenging in terms of actually yielding decent results.

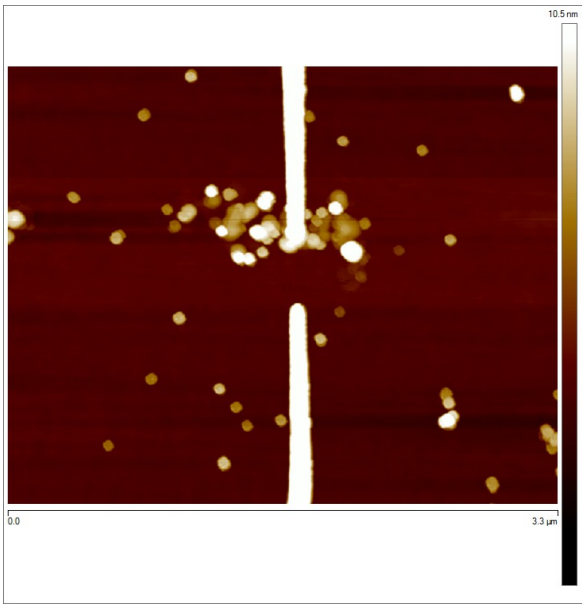

Figure 17: A sample from batch 20141008 with 1/10 dilution, 1.5 V trapping voltage, 10 MHz trapping frequency and 5 min trapping time

The above figure 17 demonstrates the results of testing the effects of a higher voltage of 1.5 V to the trapping. All of the samples that had this setting show the same results where the only thing visible is a large amount of circular particles that are approximately 5 nm high. Seemingly no origamis have attached themselves on the surface. Apparently something occurred during the trapping with these parameters since nothing similar was seen with any other samples.

4.2.4 TAE storage test

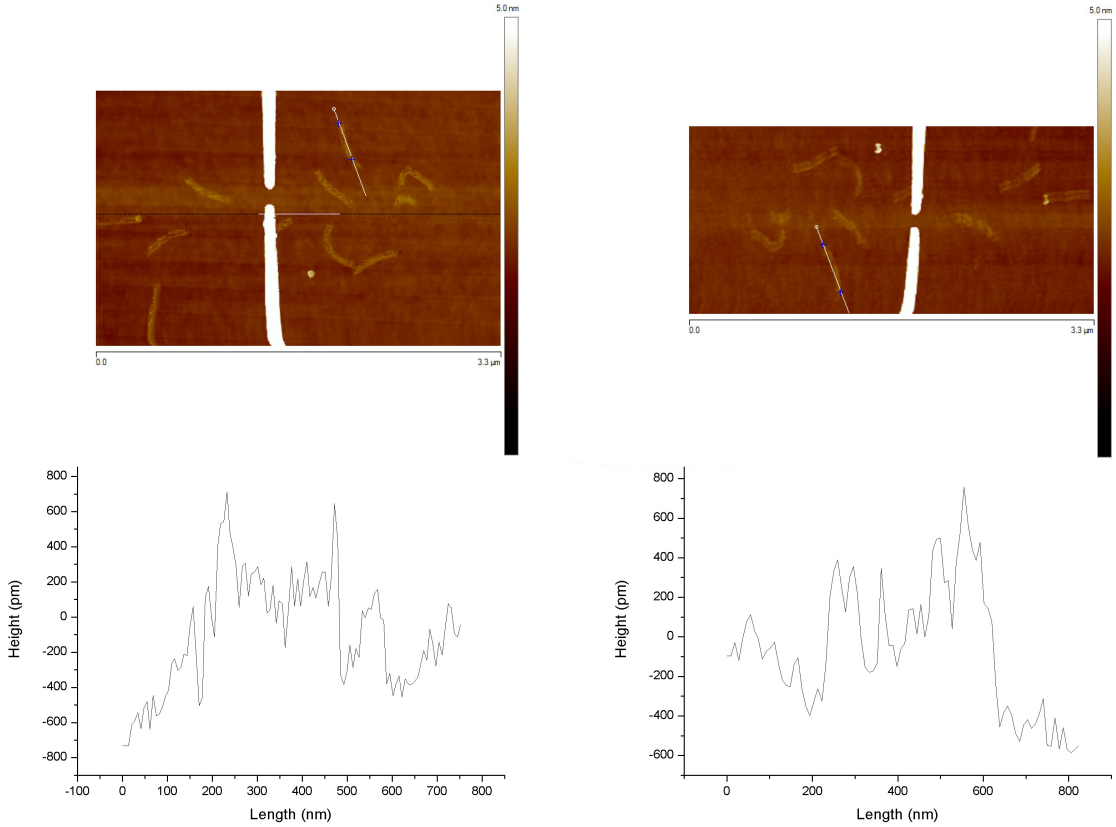

Figure 18: The effect of the TAE treatment on a sample from batch 20140717 (left: before, right: after)

As an addition to the trapping of the origamis one of the samples was placed in TAE-buffer solution overnight in order to determine whether this treatment could be used as a means to preserve the trapped origami samples during transportation as opposed to sending the samples dry. The sample before and after the TAE treatment can be seen below in figure 18. Height measurements show that after the treatment most of the origamis only had approximately half to 75% of the height that they originally had so one can conclude that this would not be an optimal method for storing.

4.2.5 General comments

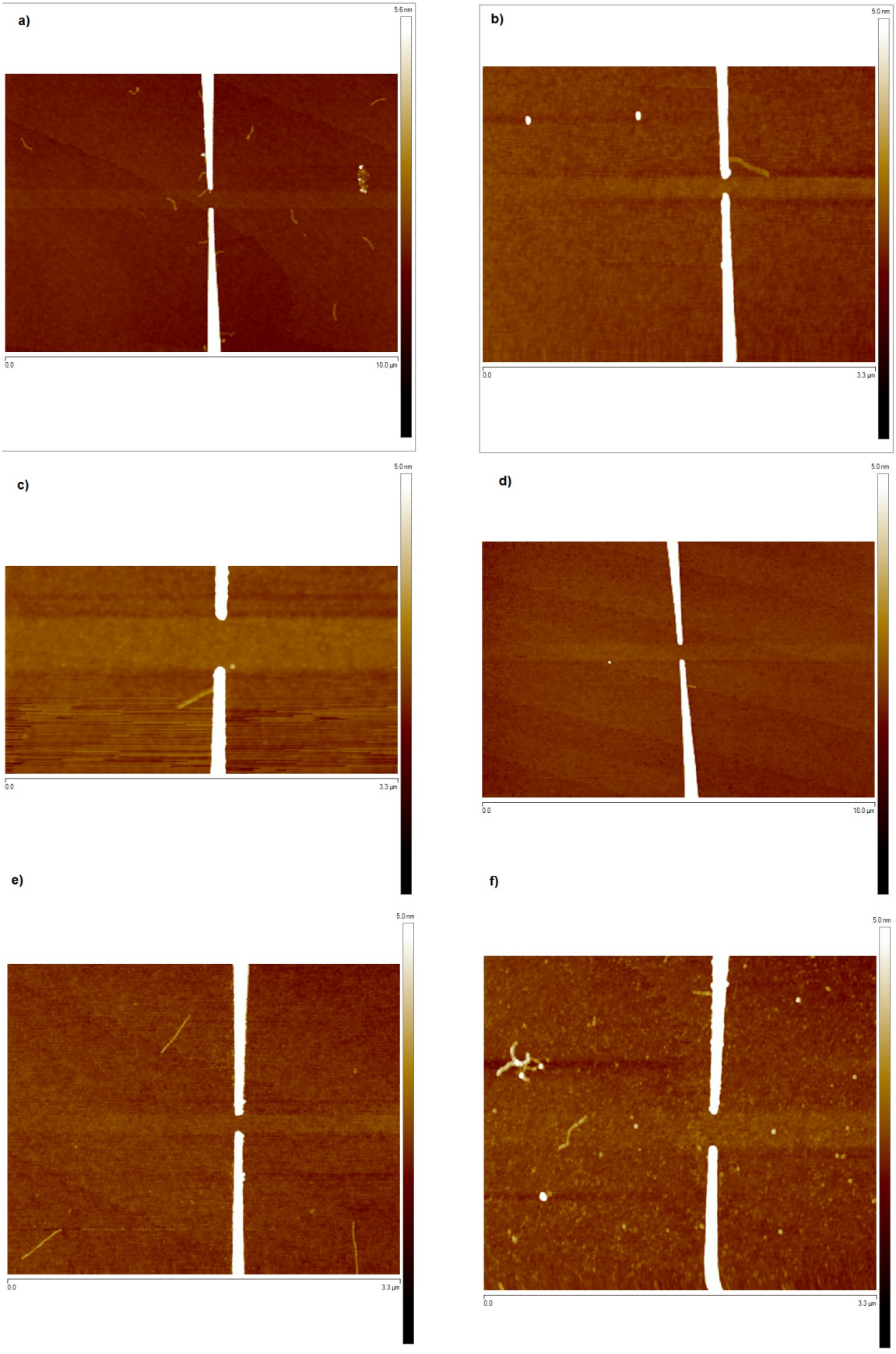

Figure 19: (previous page)a)-b): Samples from batches 20140923 and 20140806 with 1/10 dilution, 1.0 V trapping voltage, 10 MHz trapping frequency and 3/5 min trapping time respectively; c)-d): samples from batches 20141015 and 20141007 with 1/10 dilution, 1.2 V trapping voltage, 10 MHz trapping frequency and 5 min trapping time; e)-f): samples from batches 20140805 and 20140731 with 1/10 and 1/14 dilutions, 1.0 V trapping voltage, 10 MHz trapping frequency and 3 min trapping time

Figure 19 shows the most common outcomes of a trapping throughout the experiments. In most cases there was a single origami that had attached itself in one of the electrodes in the close proximity of the gap whilst neither being completely in the gap nor attached to both ends of the electrode.

During the experiments a total of 101 trapping samples were prepared, 50 with 150 nm gap electrodes and 51 with 400 nm gap electrodes. However, only eight samples out of them actually contained origamis that had been successfully trapped between the electrodes, six with 150nm gap electrodes and two with 400 nm gap electrodes. This results in a 12 % yield for 150 nm gap electrodes and ~4 % yield for 400 nm gap electrodes and an overall yield of approximately 8 % in terms of successful trappings for the whole trapping part of the work.

4.3 Discussion

The AFM imaging of the trapped samples shows clearly that the 3D-DNA origamis utilized in the experiments are rigid and durable enough to retain their structure consistently during and after the dielectrophoresis. However, many of the samples seem to exhibit at least some degree of degradation in the origamis and this is most evident in the samples which were held in the TAE buffer solution indicating that it would not be an optimal enough storage method for these molecules based on the gathered observations.

The simulations that were conducted on the model approximately representing the trapping conditions showing the distribution of the electric field and therefore the dielectric force somewhat support the results which were obtained during the trapping. Most of the origamis were naturally attached to the ends of the electrodes to the area of the greatest DEP force although some were also drawn to attach themselves along the beams of the electrodes instead of flowing towards the gap. Since the maximum of the DEP force is not constrained to the absolute tip of the electrode but also extends also along the rest of the rounded tip it could be concluded that this might be one of the reasons for the rarity of obtaining a successfully trapped origami due to them not being drawn only to the middle of the electrode gap by the dielectric force.

Furthermore, the most obvious conclusion that can be drawn from the results of the DEP-trapping is the difficulty of obtaining successfully trapped origamis when using electrodes with the larger gapsize (400 nm) as opposed to the 150 nm-gap electrodes. Since the gapsize in the larger one matches the length of the origamis it was extremely challenging to produce samples where an origami would be attached to both ends of the electrodes whereas the 150 nm-gap yielded good results with a significantly higher frequency. There was also a large amount of samples which remained completely empty after the trapping with both types of electrodes. However, given the nature of the trapping process and the fact that these occurrences were not consistent it is most probable that the empty samples were a consequence of some error in the trapping itself, such as bad contact between the electrodes and the conducting wires.

Chapter 5

Conclusions

Dielectropohretic trapping was successfully employed to position single three-dimensional DNA-origamis between nanoscale electrodes which had been fabricated lithographically in the cleanroom facilities. Although the total amount of successfully trapped single origamis was quite low, there are several observations that can be made based on the experimental part of this work as a whole. On the most basic level, the work acts as a rather explicit and clear demonstration that utilizing dielectrophoresis is indeed an unquestionably viable method for handling and manipulating nanoscale objects such as the 3D-origamis which were used here and as such the development of more sophisticated setups for dielectrophoretic trapping might be warranted. Furthermore, since the utilization of similar DNA-nanoconstructs for the purposes of molecular electronics has been a subject of intense speculation and research, the development of manipulation methods such as DEP can serve as an important step of progress in this field to contribute for the possible use of DNA as the basis for future nanoelectronic applications. Albeit DEP was used only for the positioning of origamis in this particular work, it has been shown to serve as a useful base for further research of such structures, for instance electrical conductivity measurements and other similar analysis [22,23,24].

The alignment of the origamis immobilized with DEP support the calculations of the polarizability components which were carried out earlier in Chapter 3 and are also clearly in line with the simulations of the dielectrophoretic force. Also the contribution of the geometry of the nanoelectrodes, particularly and mainly the gapsize, can be observed to have a rather large effect on the overall success of the trapping. As mentioned earlier, this was clearly seen during the experiments as it was nearly frustratingly challenging to achieve a passably trapped sample of origamis when using 400 nm gap electrodes. It can also be argued that additional variance in the trapping parameters, especially the frequency setting, could have been advantageous in order to produce more successful samples but a deliberate choice in keeping the approximately same parameters throughout the trapping was made on the grounds of using the parameters that had worked previously as the overall objective here was to produce as many successful samples as possible instead of exploring different settings and their effect on the result, although in hindsight this goal was not admittedly achieved after all.

One other factor that most probably greatly affected the trapping was the overall attachment of the nanoelectrodes onto the trapping stage which involved carefully pinning the chip in place via the electrode pads which required great accuracy and skill as the pinning was done by keeping the holders in place with tweezers as they were tightened. This was usually rather challenging and often had to be done multiple times in order to get the holders to attach precisely onto the pads. Consequently this regularly lead to at least some degree of damage being done to the electrode pads

which could have caused some disturbance to the DEP. In the cases where the trapping resulted in a completely empty sample the electrodes were recycled in a new trapping session.

As for the rest of the practical work which included the fabrication of the electrodes as well as the preparation of the origamis and the imaging of the trapped samples there were no major complications to speak of. The fabrication process and it's various phases which have been described earlier and that took place in the cleanroom, were already familiar from previous experience with working in the cleanroom with similar samples as the ones which were fabricated for this work, albeit the number of samples was much larger in this case. The fabrication of the nanoelectrodes altogether was very successful as the process steps required were relatively simple straightforward which enabled the preparation of several sample simultaneously to further fasten the process and ensured a steady supply of electrodes to be used for the trapping.

Overall the work was a success in the sense that despite the low amount of trapped the samples the number was still sufficient enough for the task and the dielectrophoresis itself which came as a new method to be learned offered not only a challenge to be tackled but also invaluable experience in the treatment, handling and manipulation of nanoscale objects in a way which was both practical and provided a functional experience of the theoretical background in action.

REFERENCES

[1] *DNA in a material world:* Nadrian C. Seeman; Nature, vol. 421, p.427-431, 2003; doi:10.1038/nature01406

[2] *DNA-based applications in molecular electronics*: Veikko Linko, Academic Dissertation for the Degree of Doctor of Philosophy, University of Jyväskylä, 2011

[3] *Nucleic acid junctions and lattices*: Nadrian C. Seeman; J. Theor. Biol. 99, 237–247, 1982; doi:10.1016/0022-5193(82)90002-9

[4] *A specific quadrilateral synthesized from DNA branched junctions*: J.-H. Chen, N.R. Kallenbach, N. C. Seeman; JACS vol. 111, p. 6402-6407, 1989; doi:10.1021/ja00198a063

[5] *Construction, Analysis, Ligation, and Self-Assembly of DNA Triple Crossover Complexes*: T. LaBean, H. Yan, J. Kopatsch, F. Liu, E. Winfree, J.H. Reif and N.C. Seeman, JACS vol. 122, p. 1848-1860, 2000; doi:10.1021/ja993393e

[6] *The Construction of a DNA Truncated Octahedron*: Y. Zhang, N.C. Seeman, JACS vol. 116, p. 1661-1669, 1994; doi:10.1021/ja00084a006

[7] *Molecular craftwork with DNA* : Nadrian C. Seeman, Chem. Intell. 1, p. 38–47, 1995; doi:10.1007/978-1-4899-7565-2_33

[8] *The Synthesis from DNA of a Molecule with the Connectivity of a Cube*: J. Chen, N.C. Seeman, Nature vol. 350, p. 631-633, 1991; doi:10.1038/350631a0

[9] *Design and self-assembly of two-dimensional DNA crystals*: E. Winfree, F. Liu, L.A. Wenzler, N.C. Seeman, Nature vol. 394, p. 539–544, 1998; doi:10.1038/28998

[10] *Folding DNA to create nanoscale shapes and patterns*: Paul W. K. Rothemund; Nature Vol

440, p. 297-302, 2006; doi:10.1038/nature04586

[11] *Self-assembly of DNA into nanoscale three-dimensional shapes*: Shawn M. Douglas, Hendrik Dietz, Tim Liedl, Björn Högberg, Franziska Graf, William M. Shih, Nature, vol. 459, p. 414-418, 2009; doi:10.1038/nature08016

[12] *Self-Assembled DNA-Based Structures for Nanoelectronics:* Veikko Linko, J. Jussi Toppari, Journal of Self-Assembly and Molecular Electronics, Vol. 1, p. 101–124, 2012; doi:10.13052/same2245-4551.115

[13] *Charge Transport in DNA-based Devices:* Danny Porath, Gianaurelio Cuniberti, Rosa Di Felice, Topics in Current Chemistry, vol. 237, p. 183-228, 2004; doi:10.1007/b94477

[14] *Itsejärjestäytyvän DNA-järjestelmän ja kultapartikkelien hybridi-sovellus yhden elektronin transistorina*: Kosti Tapio, Master's Thesis, University of Jyväskylä, 2012

[15] *Lehninger Principles of Biochemistry Third Edition*: D. L. Nelson, M. M. Cox, Worth Publishers, New York, USA, 2008; ISBN: 978-0-716-77108-1

[16] *Discovery of DNA structure and function: Watson and Crick*: Pray, L., Nature Education 1(1):100, 2008;

[17] *Nanomaterials Based on DNA*: Nadrian C. Seeman, Annu Rev Biochem, vol. 79, p. 65-87, 2010; doi:10.1146/annurev-biochem-060308-102244

[18] *DNA double-crossover molecules*: T.-J. Fu, N. C. Seeman, Biochemistry, vol. 32, p. 3211–3220, 1993; doi:10.1021/bi00064a003

[19] *DNA origami: a history and current perspective*: Jeanette Nangreave, Dongran Han, Yan Liu, Hao Yan, Current Opinion in Chemical Biology, vol. 14, p. 608-615, 2010; doi: 10.1016/j.cbpa.2010.06.182

[20] *DNA Origami: The Art of Folding DNA*: B. Saccá, C. M. Niemeyer, Angew. Chem. Int. Ed., 51, p. 58–66, 2012; doi: 10.1002/anie.201105846

[21] *Direct Mechanical Measurements Reveal the Material Properties of Three-Dimensional DNA Origami*: Dominik J. Kauert, T. Kurth, T. Liedl, R. Seidel, Nano Lett., 11, p. 5558–5563, 2011; doi:10.1021/nl203503s

[22] *Characterization of the Conductance Mechanisms of DNA Origami by AC Impedance Spectroscopy*: Veikko Linko, Seppo-Tapio Paasonen, Anton Kuzyk, Päivi Törmä, J. Jussi Toppari, Small, 5, No. 21, p. 2382–2386, 2009; doi: 10.1002/smll.200900683

[23] *Dielectrophoresis as a tool for nanoscale DNA manipulation*: S. Tuukkanen, J.J. Toppari, A. Kuzyk, P. Törmä, V.P. Hytönen, M.S. Kulomaa, International Journal of Nanotechnology, vol. 2, No. 3, p. 280-291, 2005; doi:10.1504/IJNT.2005.008065

[24] *Trapping of 27 bp–8 kbp DNA and immobilization of thiol-modified DNA using dielectrophoresis*: Sampo Tuukkanen, Anton Kuzyk, J Jussi Toppari, Hannu Häkkinen, Vesa P. Hytönen, Einari Niskanen, Marcus Rinkiö, Päivi Törmä, Nanotechnology, vol. 18, 295204, 2007; doi:10.1088/0957-4484/18/29/295204

[25] *Dielectrophoretic Trapping of DNA Origami*: Anton Kuzyk, Bernard Yurke, J. Jussi Toppari, Veikko Linko, Päivi Törmä, Small, vol. 4, p. 447–450, 2008; doi: 10.1002/smll.200701320

[26] *Trapping of DNA in Nonuniform Oscillating Electric Fields*: Charles L. Asbury, Ger van den Engh, Biophysical Journal, vol. 74, p. 1024–1030, 1998; doi:10.1016/S0006-3495(98)74027-5

[27] *Carbon Nanotubes as Electrodes for Dielectrophoresis of DNA*: Sampo Tuukkanen, J. Jussi Toppari, Anton Kuzyk, Lasse Hirviniemi, Vesa P. Hyto1nen, Teemu Ihalainen, Päivi Törmä, Nano Letters, vol. 6, no. 7, p. 1339-1343, 2006; doi:10.1021/nl060771m

[28] *Atomic Force* Microscope: G. Binnig, C. F. Quate, Ch. Gerber; Phys. Rev. Lett., 56, s. 930, 1986; doi: 10.1103/PhysRevLett.56.930

[29] *Scanning Probe microscopy: the Lab on a Tip*: Ernst Meyer, Hans Josef Hug, Roland Bennewitz, Springer, 2004, ISBN: 3540431802

[30] *Konjugoidut DNA-rakenteet: karakterisointi atomivoimamikroskoopilla*, Janne Saastamoinen, Bachelor's Thesis, University of Jyväskylä, 2014

[31] http://www.nrl.navy.mil/chemistry/6170/6177/afm_concept.php, accessed: 09.02.2014

[32] *Introduction to microfabrication*, Sami Franssila, Wiley 2004, ISBN: 978-0-470-74983-8

[33] *Invitation to the SEM world,* JEOL Ltd, 2007